REPORT DOCUMENTATION PAGE

Form Approved
OMB No. 0704-0188

1. AGENCY USE ONLY (Leave blank)	2. REPORT DATE	3. REPORT TYPE AND DATES COVERED
	8/14/98	Progress 10/97 - 8/98

4. TITLE AND SUBTITLE
Joint Services Graduate Fellowship Program
Dan Stamper-Kurn

5. FUNDING NUMBERS
N00014-98-1-0039

6. AUTHOR(S)
Dan Stamper-Kurn

7. PERFORMING ORGANIZATION NAME(S) AND ADDRESS(ES)
Research Laboratory of Electronics
Massachusetts Institute of Technology
77 Massachusetts Avenue
Cambridge, MA 02139

8. PERFORMING ORGANIZATION REPORT NUMBER

9. SPONSORING/MONITORING AGENCY NAME(S) AND ADDRESS(ES)
Office of Naval Research
Ballston Centre Tower One
800 North Quincy Street
Arlington, VA 22217-5660

10. SPONSORING/MONITORING AGENCY REPORT NUMBER
98PR00637-00

11. SUPPLEMENTARY NOTES
The view, opinions and/or findings contained in this report are those of the author(s) and should not be construed as an official Department of the Army position, policy, or decision, unless so designated by other documentation.

12a. DISTRIBUTION/AVAILABILITY STATEMENT
Approved for public release; distribution unlimited.

12b. DISTRIBUTION CODE

13. ABSTRACT *(Maximum 200 words)*

The last year, aided by the Graduate Fellowship I received from the Joint Services Electronics Program, has been a fruitful one. In the following, I summarize the progress I have made in my education and research.

19980819 010

14. SUBJECT TERMS			15. NUMBER OF PAGES
			16. PRICE CODE
17. SECURITY CLASSIFICATION OF REPORT	18. SECURITY CLASSIFICATION OF THIS PAGE	19. SECURITY CLASSIFICATION OF ABSTRACT	20. LIMITATION OF ABSTRACT
UNCLASSIFIED	UNCLASSIFIED	UNCLASSIFIED	UL

NSN 7540-01-280-5500

Standard Form 298 (Rev. 2-89)
Prescribed by ANSI Std. Z39-18
298-102

The **RESEARCH LABORATORY** *of* **ELECTRONICS**
MASSACHUSETTS INSTITUTE OF TECHNOLOGY
77 MASSACHUSETTS AVENUE
CAMBRIDGE, MASSACHUSETTS 02139-4307

14 August 1998

Colin E. Wood, ONR Code 312
ONR Program Officer
Office of Naval Research
Ballston Center Tower One
800 North Quincy Street
Arlington, VA 22217-5660

In accordance with the terms of the Office of Naval Research Fellowship No. N00014-98-1-0039, I am sending you the following material:

Type of Material:	Annual Progress Report
Title:	Joint Services Graduate Fellowship Program
Submitted by:	Dan Stamper-Kurn
Period Covered:	October 1997 - August 1998
Number of Copies:	Three plus Form 298
Distribution:	Navy Distribution List (4)

Thank you. Please contact me if you have any questions or comments.

Mary S. Greene
RLE Financial Assistant, Room 36-437

cc: D. Stamper-Kurn (1)
A.F. Favaloro, E19-750
File (1)

OSP 23970

Enclosures

Progress report from first year of JSEP fellowship (October 1997 to present)

The last year, aided by the Graduate Fellowship I received from the Joint Services Electronics Program, has been a fruitful one. In the following, I summarize the progress I have made in my education and research.

In the past year, my research has focused on Bose-Einstein condensates stored in an optical trap. Briefly, Bose-Einstein condensation is a low-temperature quantum statistical phenomenon that occurs in gases of bosons, which are particles which are allowed to coexist in a quantum state (unlike fermions, such as electrons). Once the temperature of the gas is low enough, the wavefunctions of the particles comprising the gas begin to overlap, and further cooling places nearly all the particles in the gas into a single, giant matter wave. Last year, our group made a significant advance in the field, trapping a Bose-Einstein condensate in the focus of an infrared laser beam.

This trap has allowed us to conduct four major experiments in the past year. First, we were able to place an optically trapped Bose-Einstein condensate in a large magnetic field and observe a Feshbach resonance which drastically modifies the interactions between atoms in our Bose condensates of atomic sodium. We were able to show that this resonance significantly modifies the properties of the Bose-Einstein condensates which we are studying, a tool which in the future should allow scientists to arbitarily "tune" their Bose condensed sample [S. Inouye, et al., Nature **392**, 151 (1998)].

Second, creating traps using laser light has the benefit of being able to define very narrow features in the container which holds the Bose condensate. We used this ability to demonstrate that Bose-Einstein condensates could be produced in a novel way -- just by compressing a trapped gas above the Bose-Einstein condensation transition temperature using a few milliwatts of infrared light. This project was especially satisfying as an elegant case study of thermodynamics, illuminating basic concepts such as reversibility, entropy, and phase-space density [D.M. Stamper-Kurn et al., Phys. Rev. Lett. (in press)].

Third, we used the optical trap to confine Bose-Einstein condensates that were transfered, using magnetic resonance techniques, into combinations of internal hyperfine states. Placing the trapped atoms into several atomic states leads to a new kind of quantum fluid, a three-component spinor Bose condensate. As a first exploration of this new quantum fluid, we studied the formation of spin-domains in the ground state of spinor condensates, varying the magnetic fields in which they reside [J. Stenger et al., Nature (submitted)].

Fourth, we are currently exploring Bose condensates composed of just two components, where we have discovered the spontaneous formation of metastable states in which the Bose condensate settles into a high-energy state, and cannot relax to the true ground state of the system for many

seconds. We are investigating the mechnisms by which this metastable state decays to the ground state.

Finally, in the past year I collaborated with Martin Naraschewski, a researcher at the Institute for Theoretical Atomic and Molecular Physics (ITAMP) at Harvard University, to write a theoretical paper about the finite-temperature behaviour of trapped Bose gases. The paper gives analytical expressions for the density profiles and condensate fractions of such gases which should be of immediate use to experimentalists in the field [M. Naraschewski and D.M. Stamper-Kurn, Phys. Rev. A (in press)].

In addition, I have had the opportunity to present my work and that of my colleagues. In July, I traveled to Paris, France where I visited the laboratories at the Ecole Normale Superieure, a strong center of atomic physics. There, I presented recent work during an hour-long seminar. Recently, I presented a poster at the International Conference of Atomic Physics (ICAP) in Windsor, Canada [Poster B24, ICAP16 Book of Abstracts, Windsor, Canada (1998)].

Last, I had two opportunities to advance my education as a scientist and future educator. This spring I hired an undergraduate student, Jeff C. Gore, to join our laboratory for the summer and the coming year. This gave me the opportunity to meet with many students, and to learn how to mentor newcomers in the field, an experience that will be valuable in my future career. Also, this summer, I attended the "Enrico Fermi" Summer School on Bose-Einstein condensation in Varenna, Italy, where I learned more about the field, and had the chance to meet and work with my colleagues from around the world.

In conclusion, it has been a very busy and productive year. I thank the JSEP Graduate Fellowship Program for making this work possible.

Yours,

Dan Stamper-Kurn

List of recent publications:

J. Stenger, D.M. Stamper-Kurn, M.R. Andrews, A.P. Chikkatur, S. Inouye, H.-J. Miesner, and W. Ketterle, "Optically confined Bose-Einstein condensates," J. Low Temp. Phys. (conference proceedings of Quantum Fluids and Solids, Amherst, MA 1998, in press)

J. Stenger, S. Inouye, D.M. Stamper-Kurn, H.-J. Miesner, A.P. Chikkatur and W. Ketterle. "Spin domains in ground state spinor Bose-Einstein condensates," submitted to Nature.

D.M. Stamper-Kurn, H.-J. Miesner, A.P. Chikkatur, S. Inouye, J. Stenger, and W. Ketterle. "Reversible formation of a Bose-Einstein condensate," Physical Review Letters (in press).

M. Naraschewski and D.M. Stamper-Kurn, "Analytical description of a trapped semi-ideal Bose gas at finite temperature," Physical Review A (in press).

S. Inouye, M.R. Andrews, J. Stenger, H.-J. Miesner, D.M. Stamper-Kurn and W. Ketterle, "Observation of Feshbach resonances in a Bose-Einstein condensate", Nature **392**, 151 (1998).

OPTICALLY CONFINED BOSE–EINSTEIN CONDENSATES

J. Stenger, D.M. Stamper-Kurn, M.R. Andrews, A.P.Chikkatur, S. Inouye, H.-J. Miesner, and W. Ketterle

Department of Physics and Research Laboratory of Electronics, Massachusetts Institute of Technology, Cambridge, MA 02139, USA

to appear in JLTP
12. August 1998

With an optical dipole trap it is possible to confine Bose–Einstein condensates in different hyperfine states and in arbitrary magnetic bias fields, thus overcoming two major limitations of magnetic traps. In this review paper we characterize the properties of such a dipole trap and we summarize experiments which made use of the new experimental possibilities, including the reversible formation of a Bose–Einstein condensate, the observation of Feshbach resonances in sodium and the ground state properties of spinor Bose–Einstein condensates. Finally, we present some new results on the shape of magnetically trapped and ballistically expanding condensates.

PACS numbers: 03.75 Fi, 05.30 Jp, 32.80 Pj, 64.60 -i

1. INTRODUCTION

Three years after the first observations of Bose–Einstein condensation (BEC) in dilute atomic gases[1–3] activities in this new field are still increasing, partially due to the many new experiments which have been able to generate Bose–Einstein condensates. All studies of this phenomenon have been performed in magnetic traps. These traps, in combination with rf–induced evaporation, appear ideal for cooling and trapping atoms at very low temperature and might develop into workhorses for nanokelvin atomic physics.

However, magnetic traps have severe limitations. They require large scale inhomogeneous magnetic fields which might interfere with applications in precision atom optics. For example, in the first demonstration of an atom laser,[4] coherent atomic pulses were coupled out into an inhomogeneous magnetic field, which served to confine the remaining condensate. Thus, during propagation, the pulses were exposed to Zeeman shifts. While these shifts were mitigated by producing $m_F = 0$ atoms, quadratic Zeeman shifts may preclude precision experiments on such pulses.

The unprecedented control over the motion and position of neutral atoms realized by BEC should offer major advantages for metrology. However, magnetic traps cannot trap atoms in the $m_F = 0$ state, which are preferable for atomic clocks and other precision experiments, thus limiting the use of trapped condensates for metrology.

More generally, magnetic traps can confine only weak–field seeking hyperfine states. Since the atomic ground state is always strong–field seeking, weak–field seeking states can inelastically scatter into the ground state (dipolar relaxation) resulting in heating and trap loss. This restriction to weak–field seeking states also limits the use of BEC for studies of various atomic properties which depend crucially on the hyperfine state, such as collision resonances, or for examinations of condensates composed of various combinations of hyperfine states.

These limitations have led us to the development of an all-optical trap for Bose–Einstein condensates. In this review paper, we summarize the basic properties of this trap (Section 2), and then illustrate various new possibilities for experiments on Bose–Einstein condensation, such as the following:

- Optical traps allow precise spatial (micrometer) and temporal (microseconds) manipulation of Bose–Einstein condensates. This should allow the realization of box traps, atom guides, and optical lattices. We have used the spatial resolution afforded by optical traps to create a new "dimple" trap in which BEC was created adiabatically and thus reversibly (Section 3).
- Optical traps have a new external degree of freedom: they can be operated at arbitrary external magnetic fields. We have used this feature for the observation of Feshbach resonances for strong field seeking states of sodium which cannot be confined magnetically (Section 4).
- Optical traps offer a new internal degree of freedom: the orientation of the atom's magnetic moment. This resulted in the generation of spinor condensates, condensates which populate all three hyperfine states of the $F = 1$ state of sodium (Section 5) and possess a three-component vectorial order parameter.

Finally, in Section 6, we present some unpublished quantitative results on the shape of magnetically trapped Bose-Einstein condensates, both in the trap and in ballistic expansion.

2. OPTICAL CONFINEMENT OF A BOSE–EINSTEIN CONDENSATE

Bose–Einstein condensation in an optical trap has been the ultimate goal of optical cooling and trapping techniques and has provided one motivation for the development of sub–recoil cooling techniques,[5,6] the development of various optical dipole traps,[7–11] and for pursuing Raman cooling[12,13] and evaporative cooling[14] in such traps. The highest phase space density achieved by purely optical means was a factor of 400 below that required for Bose-Einstein condensation.[12]

Rather than exclusively using optical means to create BEC, we have adopted a different approach for studying optically trapped condensates:[15] first atoms were evaporatively cooled in a magnetic trap, and then transfered into an optical trap. This approach circumvents many difficulties usually encountered with optical dipole traps, such as trap loss from heating processes which are proportional to laser power (off–resonant Rayleigh scattering), or which lead to an exponential heating with an inverse time constant proportional to the laser power (heating due to fluctuations in the intensity and position of the laser beam[16]). Since the temperature of atoms is reduced through rf–evaporation by a factor of 100, only milliwatts of laser power are needed as compared with several watts used to directly trap laser–cooled atoms. Furthermore, since the cloud shrinks while being cooled in the magnetic trap, the transfer efficiency into the small trapping volume of an optical dipole trap is increased.

The first step in this approach, the creation of a Bose-Einstein condensate in a magnetic trap, was similar to our previous work.[17] Sodium atoms were optically cooled and trapped, and transferred into a magnetic trap where they were further cooled by rf–induced evaporation. This resulted in condensates of about 20×10^6 atoms in an elongated cigar–shape trap due to our magnetic trapping configuration.

The optical trap was formed by focusing a single near–infrared laser beam into the center of the magnetic trap along the axial direction. This realized the simple single–beam arrangement for an optical dipole trap.[7–10]

The parameters of an optical dipole trap formed at the Gaussian focus of a single red–detuned laser beam are characterized by the wavelength λ of the light (and thereby the detuning from resonance δ), the total laser power P, and the beam–waist radius w_0. The trap depth is proportional to $P/w_0^2\delta$. Since trap depths on the order of a microkelvin are sufficient to trap sodium condensates, we could use infrared light ($\lambda = 985$ nm) which was far–detuned from the sodium resonance lines (at 589 nm). At this wavelength, using a typical beam radius of $w_0 = 6\,\mu$m, the trap depth is

1 μK/mW,[18] and the aspect ratio of the atom cloud is 27. Due to the large detuning of the infrared beam, the spontaneous scattering rate is small (5×10^{-3}s^{-1} per μK trap depth). None of our experiments so far has been limited by the spontaneous scattering rate – therefore there is currently no strong incentive to reduce this rate even further by using far-infrared traps[10] or blue-detuned traps.[11]

Condensates were transferred into the optical trap by holding them in a steady magnetic trap while ramping up the infrared laser power, and then suddenly switching off the magnetic trap. Nearly complete transfers of the atoms were observed, with condensate numbers in the optical trap as high as 10^7 atoms. For various experiments, we have produced pure optical traps with beam radii ranging between about 6 and 20 μm, and with infrared powers ranging from about 5 to 50 mW.

Condensates in the optical trap are usually pure, i.e. the condensate fraction is very high. This is because the optical trap has such a small volume that the number of uncondensed atoms is very low. An estimate for this number can be obtained by assuming that the temperature T of the cloud is about 1/10th of the trap depth (the optical trap has "built-in" evaporative cooling due to the limited trap depth). The number of non-condensed atoms is approximately $(k_BT/\hbar\omega)^3$, which for typical conditions is a few times 10^4 atoms, in quantitative agreement with our measurements. With a condensate of about 5 million atoms, this estimate indicates a condensate fraction of more than 99 %. "Pure" condensates in magnetic traps usually have a larger non-condensed fraction due to the smaller trapping frequencies and also due to the technical difficulty of adjusting a small trap depth using rf-induced evaporation since the trap depth is sensitive to stray magnetic fields. In the future, the condensate "purification" easily obtained with optical traps may be used in experiments to observe various predicted zero-temperature phenomena, such as collapses and revivals of collective excitations, small shifts of excitation frequencies due to quantum depletion which might otherwise be masked by finite-temperature effects, or generally for high-coherence atom lasers.

The lifetime of optically trapped condensates was studied by measuring the number of condensed atoms in time-of-flight images after a variable storage time in the optical trap. The observed loss rates per atom in the optical trap ranged from 4 s^{-1} at a peak density $n_0 = 3 \times 10^{15}$cm^{-3} to less than 1/10 s^{-1} at $n_0 = 3 \times 10^{14}$cm^{-3}. The observed decay was predominantly due to three-body recombination. The three-body loss rate constant was determined for sodium condensates as $K_3 = 1.1(3) \times 10^{-30}$cm^{6}s^{-1}. Fluctuations of the optical trapping potential did not severely limit the lifetime of the samples, which at lower densities exceeded 10 s.

From these lifetime mesurements, we can also estimate an upper limit for the heating caused by beam jitter and spontaneous scattering in the optical trap. By fitting the observed lifetime curves, we estimated a density independent loss rate of $0.03(2)\,s^{-1}$. Assuming a trap depth of about 5 μK, this implies a heating rate of about 150 nK/s, which is larger than the 25 nK/s heating rate one would expect from spontaneous scattering alone. Another estimate of this heating rate was obtained by shining the infrared light onto a sample of gas in the magnetic trap, and monitoring the temperature of the gas in this combined potential. Accounting for the fact that atoms spent only about 10% of the time in the optical potential (the rest of the time was spent in the pure magnetic potential), we arrive again at a heating rate of about 100 nK/s.

Because of the small trapping volume, and the easy availability of laser light, optically trapped condensates can be easily compressed to extremely high densities; in some of our work, condensate densities as high as 3×10^{15}cm^{-3} were observed. At such densities, the three-body recombination rate is extremely high, limiting the use of such dense samples. At the low-density end, we have produced condensates with several million atoms at densities of about 1×10^{13}cm^{-3} in a decompressed magnetic trap with a mean frequency $\bar{\omega} = 2\pi \times 7$ Hz. This wide range of possible condensate densities is impressive, especially considering that a few years ago there were many discussions whether the "BEC window" even exists.

Besides the new scientific possibilities discussed in the following paragraphs, the optical trap may become an important tool to manipulate and transport condensates. It may serve as an

"optical tweezers" to move condensates for example into optical or microwave cavities or close to surfaces.

3. REVERSIBLE FORMATION OF A BOSE–EINSTEIN CONDENSATE

In an ordinary cryostat, the experimenter can raise and lower the temperature of the sample reversibly. In contrast, evaporative cooling is irreversible due to the loss of the evaporated atoms. Even if the temperature is raised again by (internal or external) heating of the sample, the number of atoms has been reduced during the cooling stage. This reflects the fact that the trapped atoms are both the sample and the "working fluid" of the refrigerator.

If the strength of the trapping potential is changed adiabatically, one can reach higher or lower temperatures reversibly – but the density changes simultaneously in such a way that the phase space density is invariant. Thus adiabatic changes in the strength of the trapping potential cannot be used to cross the BEC transition line.

However, let us consider that one could contain a small portion of a trapped atomic sample in a vessel which is kept in thermal contact with the remaining atoms, and then use this vessel to compress the small sample. This would raise the density of a small portion of the trapped gas, but because of the thermal contact with a larger reservoir of atoms, the temperature rise would be slight. Furthermore, if such a compression were performed slowly (quasi-statically), the entropy of the gas would be unchanged, and one could reversibly (by compressing and expanding the small vessel) change the maximum phase-space density of the gas. A similar effect is achieved without such a vessel by slowly changing the shape of the trapping potential. This process conserves entropy, but can change the local phase space density.

This adiabatic (i.e. isentropic) increase in phase-space density can only occur in the presence of collisions. Without collisional thermalization, a slow adiabatic process would preserve the number of atoms in each quantum state (i.e. the Ehrenfest notion of adiabaticity) and therefore would not change the phase space density. Thus, the maximal increase in phase–space density from changes in the trapping potential will occur if such changes are made slowly with respect to the collisional (and motional) equilibration times of the trapped gas.

The possibility of adiabatic changes of the ground state population was recently shown by Pinkse and collaborators.[19] For the power-law potentials considered in their paper, the maximum increase of phase-space density is limited to a factor of 20. A more general deformation of the trapping potential can increase the phase–space density by an arbitrary factor, and an implementation of this scheme was realized using a combination of magnetic and optical forces.[20] Atoms in the magnetic trap acted as the reservoir while a small fraction of the cloud was compressed to higher densities by adding a focused red-detuned laser beam which creates a narrow potential well (a "dimple") in the center of the magnetic trap. Such small "kinks" of the trapping potential cannot be realized with ordinary magnetic traps which are produced by relatively large and distant magnets.

The increase of the phase space density was measured by cooling clouds to various temperatures slightly above the phase transition temperature T_c and determining the infrared laser power required to produce a small Bose condensate.[20] To attain the highest possible increase in phase–space density, the infrared light was increased slowly. Fig. 1 shows the increases in phase–space density. A maximum increase by a factor of 50 was obtained. Condensates were observed in clouds with temperatures as high as 5 μK. Further increases were hindered by limitations in laser power and by limits to the ramp–up time set by the various heating and loss processes in the deformed trap.

Further deformation of the potential takes the sample across the BEC phase transition. The observed condensate fractions were considerably smaller than the predictions of a model assuming non-interacting atoms, demonstrating the importance of interaction effects on the formation of the condensate. The importance of interactions is usually parametrized by a dimensionless parameter η[21] which is defined as the ratio of the mean field energy at zero temperature to the transition temperature T_c. For a harmonic trapping potential with mean oscillation frequency ω, the mean field energy is proportional to $\omega^{6/5}$ and $T_c \propto \omega$, leading to $\eta \propto \omega^{1/5}$. Due to this weak dependence

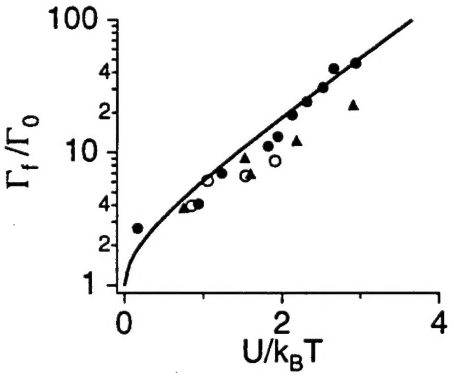

Fig. 1. Phase-space density increase to reach BEC vs. normalized well-depth (from Ref. 20). Various trap settings were used for the the mean trapping frequency ω and the beam waist w_0: $\omega = 2\pi \times 100$ Hz, $w_0 = 9\,\mu$m (triangles); $\omega = 2\pi \times 100$ Hz, $w_0 = 18\,\mu$m (open circles); and $\omega = 2\pi \times 33$ Hz, $w_0 = 18\,\mu$m (closed circles). The solid line gives theoretical prediction.

(and also a weak dependence on the number of trapped atoms), all experiments done so far realized η parameters in the range of 0.3 to 0.4[21] and did not show evidence for interaction effects.

In contrast, the "dimple" trap is characterized by two trapping frequencies, one for the broad magnetic trapping potential which determines T_c, and one for the bottom of the optical trapping potential which confines the condensate and determines its mean field energy. Thus, the parameter η can be greatly increased, exceeding the values reached in purely magnetic traps by a factor of about hundred. Fig. 2 shows the ballistic expansion of a condensate which is clearly faster than the expansion of the thermal cloud, which means that, even for small condensate fractions, the mean field energy can exceed k_BT.

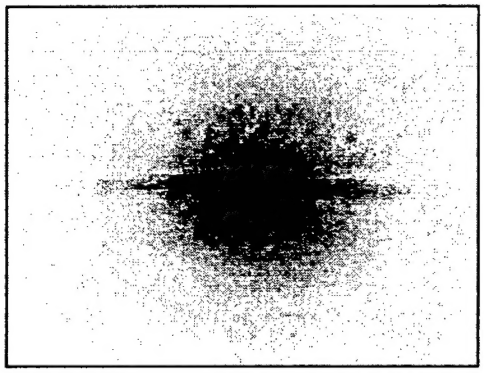

Fig. 2. In the dimple trap interaction effects are greatly enhanced and the meanfield energy of the condensate can exceed the thermal energy. Shown is the ballistic expansion of the cloud 50 ms after the release from the "dimple" trap. The disc–like expansion of the condensate is faster than the isotropic thermal expansion.

The reversibility of crossing the BEC phase transition was demonstrated by preparing a magnetically trapped cloud just above T_c. We then sinusoidally modulated the power of the infrared light at 1 Hz, between zero and 7 mW. This modulation frequency was significantly smaller than the magnetic trap frequencies ($\omega_r = 2\pi \times 48$Hz and $\omega_z = 2\pi \times 16$ Hz). These low frequencies and a large optical focus ($w_0 = 18\ \mu$m) were used to minimize trap loss due to inelastic collisions.

During the first seven condensation cycles the condensate fraction oscillated between zero and 6 %, as shown in Fig. 3; later probing showed repeated condensation for at least 15 cycles. The peak of these oscillations decreased slowly in time due to a small heating rate resulting from slight instabilities in our optical setup.

This method of creating condensates provides insight into their formation, which was recently studied experimentally[22] and theoretically.[23] For example, in the experiment described above, the condensate fraction was found to lag about 70 ms behind the modulation of the laser power, which is a measure for the formation time. Note that this formation time is much smaller than the 1 s timescale for changing the trapping potential, thus confirming that the condensation was done quasi–statically.

Compared to evaporative cooling in magnetic traps, deformation of the trapping potential offers several advantages for the study of the BEC phase transition. For example, in a previous study

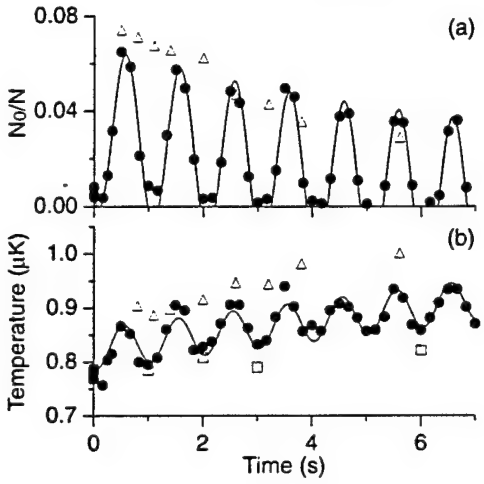

Fig. 3. Adiabatic cycling through the phase transition (from Ref. 20). Shown is the condensate fraction (a) and the temperature (b) versus time for the case of a modulated infrared beam (closed circles), an infrared beam ramped up to a constant power (open triangles), and no infrared light (open squares). The solid lines are guides to the eye.

of the BEC formation process, a sudden spatial truncation of the thermal cloud by an rf–sweep was used to quench the system into BEC.[22] To clearly interpret the results of such a truncation, one either has to model the process of rf–truncation, or use a very low density cloud to ensure a separation of the time scales for truncation and thermalization. In contrast, the deformation of the trap using infrared light can be applied in microseconds and its characterization is straightforward. In one such experiment, we switched on the infrared light instantly, and observed condensation on time scales much faster than the oscillation periods in the magnetic trap and along the weakly confining axis of the optical trap, as shown in Fig. 4. The resulting condensates showed striations in time–of–flight images, indicating that the condensates formed into excited states of the deformed potential. Such studies of shock–condensation might give new insight into the formation of quasi–condensates and condensation into excited states.[24,25]

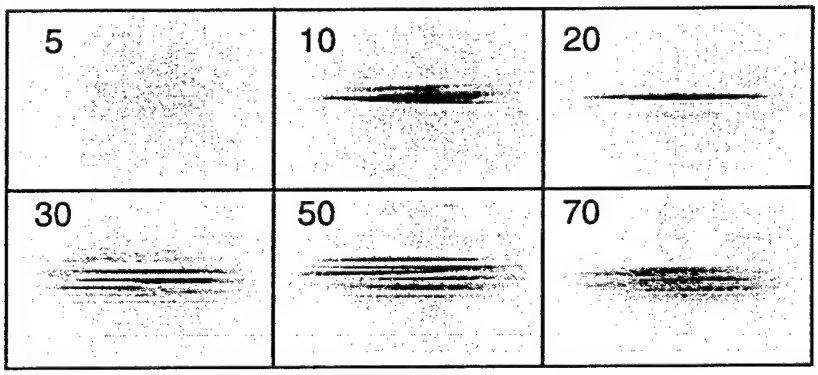

Fig. 4. Formation of the condensate after a sudden switch on of the IR laser. Shown is the cloud after a ballistic expansion of 50 ms for various dwell times in the "dimple" trap (numbers given in ms). A small condensate fraction is already visible after 10 ms. During the first 50 ms of formation the condensate shows gross striations which disappear at longer dwell times. This type of studies could be suitable for observing the formation of quasi-condensates, where phase fluctuations might lead to striations in the ballistic expansion.

Also, deformation of the trapping potential greatly extended the range of transition temperatures which we can easily access. The compression of the thermal cloud by the light potential resulted in extreme critical densities $n_c \approx 5 \times 10^{14}\,\mathrm{cm}^{-3}$ and critical temperatures $T_c \approx 5\,\mu\mathrm{K}$. At low densities, crossing the BEC transition in a purely magnetic trap is hindered by ineffectiveness of rf–evaporation (caused by the sagging of the cloud due to gravity) and the technical difficulties of controlling very small trap depth with rf– and magnetic fields. However, using our method of

deforming the potential, we could shine the infrared laser into a decompressed magnetic trap ($\omega = 7$ Hz) and cross the transition at $n_c \approx 2 \times 10^{12}\,\mathrm{cm}^{-3}$ and $T_c \approx 100$ nK.

Reversible cooling by adiabatic deformation of the trapping potential is achieved by a modification of the density of states. When a potential dimple is added to a broad harmonic oscillator potential, it lowers the energy of the ground state, but affects very few of the excited states of the system. As the well-depth is increased, the ground state energy reaches the chemical potential, and BEC occurs. An alternative way of describing this process is to first compress the whole cloud by increasing the harmonic oscillator frequency to the value at the bottom of the dimple, and then opening up the potential to the original broad harmonic oscillator potential outside a small central area. The last step increases the density of states at high energy, and as a result, elastic collisions preferably populate these states. This is very similar to evaporative cooling where rf-induced spin-flips couple higher lying states to the continuum leading to a net collisional transfer of atoms to these states. The major difference is that in evaporative cooling no equilibrium is established between the evaporated atoms and the trapped atoms, whereas in the case of the deformed potential, the whole cloud stays in thermal equilibrium.

4. OBSERVATION OF FESHBACH RESONANCES IN A BOSE–EINSTEIN CONDENSATE

All the essential properties of Bose condensed systems – the formation and shape of the condensate, the nature of its collective excitations and statistical fluctuations, the formation and dynamics of solitons and vortices – are determined by the strength of the atomic interactions. In contrast to the situation for superfluid helium, these interactions are weak, permitting the phenomena to be theoretically described from "first principles". Furthermore, in atomic gases the interactions can be altered, for instance by employing different species, changing the atomic density, or, as we discuss here, merely by varying a magnetic field.

At low temperatures, the interaction energy in a cloud is proportional to the density and a single atomic parameter, the scattering length a, which depends on the quantum-mechanical phase shift in an elastic collision. It has been predicted that the scattering length can be modified by applying external magnetic,[26–30] optical[31,32] radio-frequency (rf),[33] and electric fields.[34] Those modifications are only pronounced near zero-energy resonances, either shape resonances[34] or "Feshbach resonances".[35] A Feshbach resonance occurs, when a quasibound molecular state has nearly zero energy and couples resonantly to the free state of the colliding atoms. In a time-dependent picture, the two atoms are transferred to the quasibound state, "stick" together and then return to an unbound state. Such a resonance strongly affects not only the scattering length (elastic channel), but also inelastic processes such as dipolar relaxation[26,27] and three-body recombination. Feshbach resonances have so far been studied at much higher energies[36] by varying the collision energy. In our recent work[37] we have shown that they can be tuned to zero energy to be resonant for ultracold atoms. The different magnetic moments of the free and quasibound states allowed us to tune these resonances with magnetic fields, and as a result, minute changes in the magnetic field strongly affected the properties of a macroscopic system.

Above and below a Feshbach resonance, the scattering length a covers the full continuum of positive and negative values. It was predicted to vary dispersively as a function of magnetic field B:[28]

$$a = \tilde{a}\left(1 + \frac{\Delta}{B_0 - B}\right) \tag{1}$$

where Δ parameterizes the width of the resonance at $B = B_0$, and $\tilde{a}$ is the scattering length away from the resonance. Feshbach resonances should allow the realization of condensates over a wide range of interaction strengths. By setting $a \approx 0$, one can create a condensate with essentially non-interacting atoms, and by setting $a < 0$ one can make the system unstable and observe its collapse. Rapid tuning of an external magnetic field around a Feshbach resonance will lead to

sudden changes of the scattering length. This opens the door to studies of new dynamical effects such as novel forms of collective oscillations or the sudden collapse of a large condensate when the scattering length is switched from positive to negative.[38] Feshbach resoncances have recently been also observed in rubidium, in photoassociation spectroscopy of laser-cooled atoms,[39] and as a resonance in the elastic scattering cross section of magnetically trapped atoms.[40]

Theoretical calculations predicted Feshbach resonances for sodium only for hyperfine states which cannot be magnetically trapped.[28,41] The optical trap described above was therefore indispensible for this study. After optically trapped Bose-Einstein condensates were produced as described in Section 2, they could be transfered to the $m_F = +1$ state with an adiabatic rf-sweep, and were then exposed to a bias field up to $\sim$ 1200 G. The inhomogeneity of the bias field destabilized the optical trap in the axial direction and therefore required the use of two additonal "endcaps" of far-off-resonant blue-detuned laser light.[37]

When the magnetic field is swept across a Feshbach resonance one would expect to lose a condensate due to an enhanced rate of inelastic collisions (caused either by the collapse in the region of negative scattering length or by an enhanced rate coefficient for inelastic collisions). This was used to locate three resonances near 853 G, 907 G, and 1195 G by the sudden onset of trap loss.

In order to measure the variation of the scattering length around the resonance near 907 G, we determined the interaction energy of a trapped condensate. This was done by suddenly switching off the trap, allowing the stored interaction energy to be converted into the kinetic energy of a freely expanding condensate and measuring it in time-of-flight absorption imaging. The interaction energy is proportional to the scattering length and the average density of the condensate. Both quantities can be directly extracted from time-of-flight images, and the results for the scattering length are shown in Fig. 5 together with the theoretical prediction[41] of a $\Delta = 1$ G wide resonance. The data clearly displays the predicted dispersive shape and shows evidence for a variation in the scattering length by more than a factor of ten.

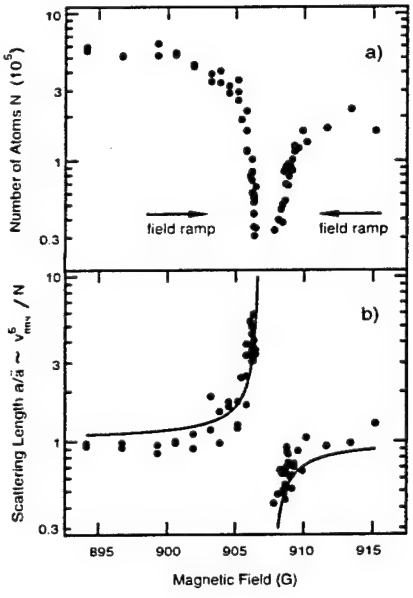

Fig. 5. Observation of the Feshbach resonance at 907 G using time-of-flight absorption imaging (from Ref. 37). Fig. a) shows the number of atoms in the condensate versus magnetic field. Field values above the resonance were reached by quickly crossing the resonance from below and then approaching from above slowly. Fig. b) shows the normalized scattering length $a/\bar{a} \propto v_{rms}^5/N$ calculated from the released energy, together with the predicted shape (Eq. 1, solid line). The values of the magnetic field in the upper scan relative to the lower one have an uncertainty of less than 0.5 G.

The trap losses observed around the Feshbach resonances merit further study since they might impose practical limits on the possibilities for varying the scattering length. An increase of the dipolar relaxation rate near Feshbach resonances has been predicted,[26,27] but for atoms in the lowest hyperfine state no such inelastic binary collisions are possible. Therefore, the observed trap loss for the resonances in the $|F = 1, m_F = +1\rangle$ state is probably due to three-body collisions. In

this case the loss rate is characterized by the coefficient K_3, defined as $\dot{N}/N = -K_3 \langle n^2 \rangle$. So far, there is no theoretical work on K_3 near a Feshbach resonance. An analysis based on Fig. 5 shows that K_3 increased on both sides of the resonance, because the loss rate increased while the density decreased or stayed constant. The inferred increase of K_3 is fairly dramatic (up to five orders of magnitude). The trap loss prevented the study of the region with negative scattering length: the condensate was lost before this region could be reached. A lifetime of the condensate of at least one oscillation period in the trap is required to observe the collapse of an unstable condensate. For the sodium resonances presented here, this requires lower density condensates and therefore an optical trap with a larger volume. Whether the observed enhancement of the three-body recombination rate is generic for any Feshbach resonance or only specific to sodium remains to be seen – both experimental and theoretical work along these lines is in progress.

Our observation of the dispersive variation of the scattering length confirms the theoretical predictions about "tunability" of the scattering length with the prospect of "designing" atomic quantum gases with novel properties; e.g. to create ideal Bose-Einstein condensates with nearly zero scattering length and to obtain a detailed picture of the collapse of a condensate with negative scattering length which is so far not fully understood. Tuning the scattering length can also be used to vary interactions between different species[42] and thus control the phase diagram of multi-component condensates, possibly switching from interpenetrating superfluids to phase separation.[43] Feshbach resonances may also be important in atom optics, for modifying the atomic interactions in an atom laser, or more generally, for controlling non-linear coefficients in atom optics with coherent beams of atoms.

5. SPINOR BOSE–EINSTEIN CONDENSATES IN OPTICAL TRAPS

Bose-Einstein condensates in magnetic traps are described by a scalar order parameter similar to the spinless superfluid ^{4}He. Even though alkali atoms have angular momentum, the spin orientation is not a degree of freedom because the atomic spin adiabatically follows the magnetic field. Spin flips lead to untrapped states and are therefore a loss process. In contrast, an optical trap confines atoms in all spin states, opening the possibility to study spinor condensates which have the spin orientation as a new degree of freedom. They represent a system with a vector order parameter instead of a scalar. A variety of new phenomena is predicted,[44–46] such as spin textures, propagation of spin waves and coupling between superfluid flow and atomic spin.

Other systems which go beyond the description with a single scalar order parameter are condensates of two different hyperfine states of ^{87}Rb confined in magnetic traps. Recent experimental studies have explored the spatial separation of the two components[47,48] and their relative phase.[49] Several theoretical papers describe their structure[43,50–55] and their collective excitations.[56–59]

Compared to these two-component condensates, spinor condensates have several new features including the multi-component vector character of the order parameter and the changed role of spin relaxation collisions which allow for population exchange among hyperfine states without trap loss. In contrast, in the ^{87}Rb experiments trap loss due to spin relaxation severely limits the lifetime.

We have recently studied the equilibrium state of spinor condensates in an optical trap.[60] In an $F=1$ spinor condensate subject to spin relaxation, two $m_F=0$ atoms can collide and produce a $m_F=+1$ and a $m_F=-1$ atom and vice versa. The most dramatic effect is seen when we start out with a condensate in a pure m=0 state. Depending on the external magnetic field, we observed the formation of three domains of $m_F=+1, 0$, and -1 atoms.

The experimental study of spinor condensates requires techniques to selectively prepare and probe condensates in arbitrary hyperfine states. The first step was the preparation of $m_F=-1$ condensates in an optical trap as described above. Arbitrary populations of the three hyperfine states were prepared using rf–transitions (Landau–Zener sweeps) similar to our earlier work.[4] At a bias field of about 40 G the transitions from $m_F=-1$ to $m_F=0$ and from $m_F=0$ to $m_F=+1$ differ in frequency by about 0.9 MHz due to the quadratic Zeeman shift and they could be driven separately. Without this frequency difference rf–fields would only rotate the spin vector and it

would not be possible to produce pure $m_F = 0$ condensates. After the spin preparation, a bias field B_0 and a field gradient B' were applied for a variable amount of time (as long as 30 s), during which the atoms relaxed towards their equilibrium distribution. The bias field was varied between 20 mG and 500 mG and the gradients between ± 70 mG/cm.

Both the spatial and hyperfine distributions were observed by time–of–flight absorption imaging. For this, the optical trap was suddenly switched off and the atoms were allowed to expand. Due to the large aspect ratio, the expansion was almost purely in the radial directions. A magnetic field gradient, which was applied after 5 ms time–of–flight, acted as a Stern-Gerlach filter and separated the three spin components. In this manner, a single time–of–flight image provided both a spatial and a spin–state description of the trapped cloud. After a total time–of–flight of 25 ms the atoms were pumped into the $F = 2$ hyperfine state and observed using the $m_F = +2$ to $m_F = +3$ cycling transition. This technique assured the same transition strength for atoms originating from different spin states.

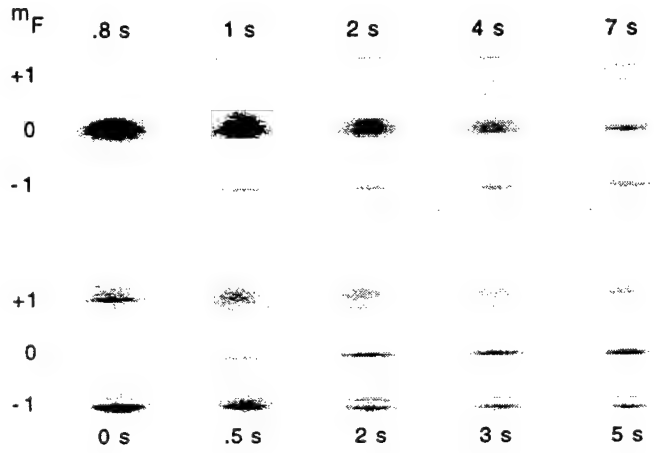

Fig. 6. Absorption images of spinor condensates released from the optical trap, after 25 msec of ballistic expansion (from Ref. 60). The different m_F states were separated by an axial field gradient. The images taken after various dwell times in the trap show how the atoms evolved into the same equilibrium distribution although they were initially prepared in a pure $m_F = 0$ state (upper row) or in equally populated $m_F = \pm 1$ states (lower row). The bias field during the dwell time was $B_0 = 20$ mG and the gradient was $B' = 11$ mG/cm. The height of the images is 2.7 mm.

Fig. 6 shows a sequence of images with different dwell times in the optical trap. Starting with the pure $m_F = 0$ component (upper series) or with a 50–50 mixture of the $m_F = \pm 1$ components (lower series), the same equilibrium distribution was reached.

Comparison of images like those in Fig. 6 to a theoretical model revealed that the spin-dependent interaction $c\vec{F}_1 \cdot \vec{F}_2$ between two sodium atoms in the $F = 1$ state is anti–ferromagnetic (i.e. $c > 0$). Furthermore, the experimental results showed clear evidence for the miscibility of $m_F = -1$ and $m_F = +1$ components and the immiscibility of $m_F = \pm 1$ and $m_F = 0$. This opens the possibility for detailed studies of miscible and immiscible multi–component condensates.

The anti–ferromagnetic energy was estimated to be 2.5 nK in our condensates. It is interesting to note that the optically trapped samples in which the domains were observed were at a temperature of the order of 100 nK, far larger than the anti–ferromagnetic energy. Thus the formation of spin domains occurs only in a Bose–Einstein condensate. This illustrates a new regime accessible with Bose–Einstein condensates: a few nK energy are responsible for spin domains of a gaseous Bose–condensed cloud.

The dynamics of domain formation deserves further study. For example we have placed a two–component condensate in a state with higher energy than the groundstate, representing a

non-equilibrium configuration which is metastable for many seconds. We are currently studying the conditions for this metastability and the mechanisms by which the equilibrium finally is approached.

6. THE SHAPE OF MAGNETICALLY TRAPPED BOSE-EINSTEIN CONDENSATES

Finally, we would like to present some unpublished results from our work with magnetically trapped condensates: *in situ* density profiles of atomic clouds above and below the BEC phase transition which illustrate the onset of a *spatial* condensation of atoms, and measurements on condensates released from the magnetic trap and allowed to freely expand, which confirm the mean-field description of such condensates.

Bose-Einstein condensation in a homogeneous system is appropriately described as "condensation in momentum space"[61] because it does not lead to spatial separation between the normal component and the condensate. However, in any inhomogeneous potential – i.e. atom traps – the condensate and the normal fraction are spatially separated.[61,62] This occurs because the condensate atoms settle into the areas of lowest potential energy where the ground state lies. *In situ* images of such a separation were first taken with alkali atom gases using the dark-ground imaging technique, which clearly distinguished the high-density of the condensate from the background thermal cloud in a magnetically trapped sample.[63] Since then, the phase-contrast technique has been used for *in situ* studies of the condensate, using the non-destructive character of such non-resonant imaging to image the condensate repeatedly and measure dynamical properties such as the propagation of Bogoliubov sound,[64] the formation of a condensate,[22] and collective excitations at non-zero temperatures.[65] In such images, the signal which is obtained is linear, rather than quadratic, in the column density of the gaseous sample, and thus clear images with a large dynamic range are obtained.

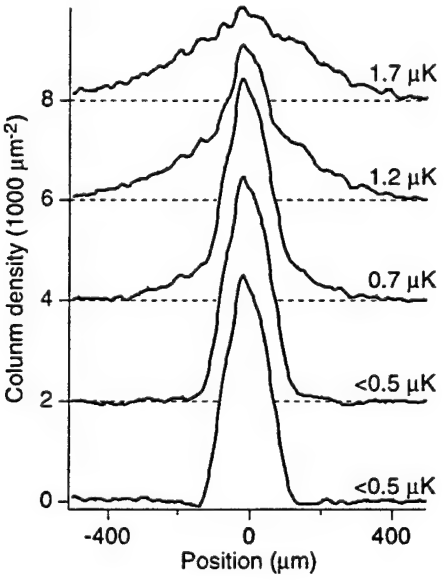

Fig. 7. Bose-Einstein condensation in coordinate space. Traces show axial profiles of column densities of Bose gases from phase-contrast images. Trapping frequencies are 17(1) Hz axially and 230(20) Hz radially. Temperatures are determined from fits to the thermal tails. As the temperature is lowered, the thermal cloud is depleted, and atoms accumulate in the Bose condensate.

In Fig. 7, we present a series of profiles of column densities obtained from phase-contrast images of clouds above and below the BEC phase transition. The profiles are taken along the axis in which the condensate is longest. As in our other work, such images are taken with light which is 1.7 GHz red-detuned from the D_2 resonance of a magnetically trapped sample of sodium atoms in the $|F = 1, m_F = -1\rangle$ hyperfine state. While such images are non-destructive, the five traces shown in the figure are taken from different clouds, each of which was brought to a different temperature. One can clearly see that as the temperature is lowered from 1.8 μK to 1.2 μK and below, a high-density peak arises in the center of the cloud, corresponding to the accumulation

of condensate atoms at the bottom of the confining potential well. As the temperature is lowered further, to below 0.5 μK, the "thermal tails" of the central condensate peak disappear, indicating that almost all the remaining atoms form a Bose–Einstein condensate, which contains on the order of 10^7 atoms. The width of the condensate (almost 300 μm at low temperatures in this figure) is determined by its mean–field energy: at the edge of the condensate, the trap potential energy and the mean–field energy (chemical potential) of the condensate are equal. In comparison, the non–interacting ground state in a harmonic well with a trap frequency of 17 Hz (as in the figure) has a half–width of 5 μm – a clear indication of the importance of interactions in the static and dynamical properties of such condensates, and a clear justification for the use of the Thomas-Fermi approximation.

The temperature of each cloud, as indicated on each trace, is determined by fitting a Gaussian function to the wings of the density profile, away from the central condensate peak. The width of this Gaussian can be combined with the trapping frequency in the axial direction (which can be determined precisely by *in situ* measurements) to obtain the temperature. However, as indicated for the last two traces in the figure, temperatures which are lower than the chemical potential are difficult to measure by this method, because the extent of the thermal cloud and of the condensate are similar, and furthermore the non–condensed fraction at such low temperatures is extremely small. This poses a limitation on studying low–temperature properties of condensates (as discussed in Section 2).

This problem may be somewhat obviated by measuring temperatures in anisotropic traps by time–of–flight techniques. Since condensates from such traps expand primarily in only one (pancake condensates) or two (cigar-shaped condensates) directions while the thermal cloud expands isotropically, a clearer spatial separation of the two components occurs along the axis of slow condensate expansion, allowing for a temperature measurement.

This anisotropic expansion of Bose–Einstein condensates from harmonic magnetic traps has been investigated experimentally and theoretically.[66] The anisotropy was one of the distinguishing characteristics of Bose–Einstein condensates which allowed for their identification in early BEC experiments, and allows for the clear separation between the condensed and non–condensed fractions. The shape of the condensate in time–of–flight arises from the anisotropy of a trapped condensate for two reasons. First, the shape of the trapped condensate implies an anisotropic momentum distribution in the trap, thus, in a interaction–free time–of–flight, this momentum distribution should yield an anisotropic expanding cloud. However, in the presence of interactions, this kinetic energy effect is much smaller than the mean–field energy of the condensate; this energy is released preferentially along the narrowest directions of the trapped condensate and is converted to kinetic energy. For large condensates, this expansion is well–described by the Gross-Pitaevskii equation solved in the Thomas-Fermi approximation[67–71] wherein the evolution is described by a simple scaling solution of the original parabolic density profile in the harmonic trap.

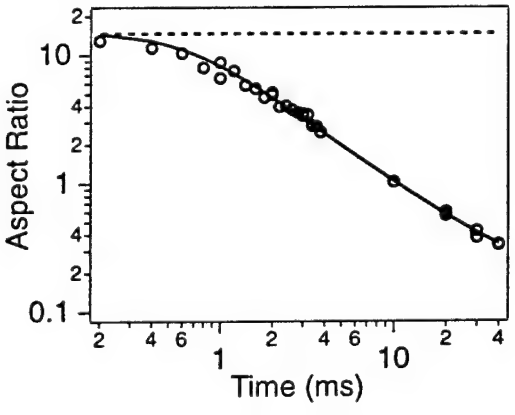

Fig. 8. Aspect ratio (axial to radial widths) of expanding Bose condensates. Data collected for times less than 10 ms were taken in phase-contrast imaging due to the high optical density. Other data were taken with absorption imaging. The dashed line indicates the ratio of trapping frequencies of 248(1) Hz radially and 16.23(3) Hz axially. The solid line gives the prediction of Ref. 69.

We probed this free–evolution using a combination of phase–contrast (short time–of–flight)

and absorption (long time–of–flight) imaging. The measured aspect ratios of a freely–expanding condensate are presented in Fig. 8. The data clearly show two steps in the expansion. First, during the first millisecond or so, the atoms are accelerated radially by the stored mean–field energy. Then, the atoms travel ballistically, expanding the condensate in the radial direction at a constant velocity, while the axial expansion is nearly absent due to the large original axial extent of the cloud. The final stage of the expansion, where the cloud reaches a final, asymptotic aspect ratio, occurs only at times larger than our accessible range of times–of–flight. The data are presented along with a predicted evolution[69] for which the only input is the axial and radial trap frequencies which we measured precisely with repeated *in situ* imaging. The agreement between theory and experiment is excellent, and provides convincing proof for the validity of the Gross-Pitaevskii equation to describe large–amplitude dynamics.

ACKNOWLEDGMENTS

This work was supported by the Office of Naval Research, NSF, Joint Services Electronics Program (ARO), NASA, and the David and Lucile Packard Foundation. J.S. would like to acknowledge support from the Alexander von Humboldt-Foundation, D.M.S.-K. from the JSEP Graduate Fellowship Program, and A.P.C. from the NSF. M.R.A. is now at Bell Labs, Murray Hill.

REFERENCES

1. M.H. Anderson *et al.*, *Science* **269**, 198 (1995).
2. K.B. Davis *et al.*, *Phys. Rev. Lett.* **75**, 3969 (1995).
3. C.C. Bradley, C.A. Sackett, and R.G. Hulet, *Phys. Rev. Lett.* **78**, 985 (1997), see also: C.C.Bradley *et al.*, *Phys. Rev. Lett.* **75**, 1687 (1995).
4. M.-O. Mewes, M.R. Andrews, D.M. Kurn, D.S. Durfee, C.G. Townsend, and W. Ketterle; *Phys. Rev. Lett.* **78**, 582 (1997).
5. A. Aspect *et al.*, *Phys. Rev. Lett.* **61**, 826 (1988).
6. M. Kasevich and S. Chu, *Phys. Rev. Lett.* **69**, 1741 (1992).
7. S. Chu, J.E. Bjorkholm, A. Ashkin, and A. Cable, *Phys. Rev. Lett.* **57**, 314 (1986).
8. W.D. Phillips, in *Laser Manipulation of Atoms and Ions*, edited by E. Arimondo, W.D. Phillips, and F. Strumia, Proceedings of the International School of Physics "Enrico Fermi", Course CXVIII (North-Holland, Amsterdam, 1992) p. 289.
9. J.D. Miller, R.A. Cline, and D.J. Heinzen, *Phys. Rev. A* **47**, R4567 (1993).
10. T. Takekoshi and R.J. Knize, *Optics Lett.* **21**, 77 (1996).
11. T. Kuga *et al.*, *Phys. Rev. Lett.* **78**, 4713 (1997).
12. H.J. Lee *et al.*, *Phys. Rev. Lett.* **76**, 2658 (1996).
13. A. Kuhn, H. Perrin, W. Hänsel, and C. Salomon, in *Ultracold Atoms and Bose-Einstein-Condensation*, edited by K. Burnett, OSA Trends in Optics and Photonics Series, Vol. 7 (Optical Society of America, Washington D.C., 1996) p. 58.
14. C.S. Adams *et al.*, *Phys. Rev. Lett.* **74**, 3577 (1995).
15. D.M. Stamper-Kurn, M.R. Andrews, A.P. Chikkatur, S. Inouye, H.-J. Miesner, J. Stenger, and W. Ketterle, *Phys. Rev. Lett.* **80**, 2027 (1998).
16. T.A. Savard, K.M. O'Hara, and J.E. Thomas, *Phys. Rev. A* **56**, R1095 (1997).
17. M.-O. Mewes *et al.*, *Phys. Rev. Lett.* **77**, 416 (1996).
18. 25% of the trap depth comes from the "counter-rotating" term usually neglected in the rotation-wave approximation.
19. P.W.H. Pinkse *et al.*, *Phys. Rev. Lett.* **78**, 990 (1997).
20. D.M. Stamper-Kurn, H.-J. Miesner, A.P. Chikkatur, S. Inouye, J. Stenger, and W. Ketterle, *Phys. Rev. Lett.* accepted for publication on Sept. 14 (1998).
21. S. Giorgini, L.P. Pitaevski, and S. Stringari, *J. Low Temp. Phys.* 109, 309 (1997).
22. H.-J. Miesner *et al.*, *Science* **279**, 1005 (1998).
23. C.W. Gardiner, P. Zoller, R.J. Ballagh, and M.J. Davis, *Phys. Rev. Lett.* **79**, 1793 (1997).
24. Y. Kagan, B.V. Svistunov, and G.V. Shlyapnkov, *Sov. Phys. JETP* **75**, 387 (1992).
25. C.W. Gardiner *et al.*, preprint cond-mat/9801027 (unpublished).
26. E. Tiesinga, A.J. Moerdijk, B.J. Verhaar, and H.T.C. Stoof, *Phys. Rev. A* **46**, R1167 (1992).

27. E. Tiesinga, B.J. Verhaar, and H.T.C. Stoof, *Phys. Rev. A* **47**, 4114 (1993).
28. A.J. Moerdijk, B.J. Verhaar, and A. Axelsson, *Phys. Rev. A* **51**, 4852 (1995).
29. J.M. Vogels, C.C. Tsai, R.S. Freeland, S.J.J.M.F. Kokkelmans, B.J. Verhaar and D.J. Heinzen, *Phys. Rev. A* **56**, R1067 (1997).
30. H.M.J.M. Boesten, J.M. Vogels, J.G.C. Tempelaars, and B.J. Verhaar, *Phys. Rev. A* **54**, R3726 (1996).
31. P.O. Fedichev, Y. Kagan, G.V. Shlyapnikov, and J.T.M. Walraven, *Phys. Rev. Lett.* **77**, 2913 (1996).
32. J.L. Bohn and P.S. Julienne, *Phys. Rev. A* **56**, 1486 (1997).
33. A.J. Moerdijk, B.J. Verhaar, and T.M. Nagtegaal, *Phys. Rev. A* **53**, 4343 (1997).
34. M. Marinescu and L. You, *Phys. Rev. Lett.*, submitted.
35. H. Feshbach, *Ann. Phys.* **19**, 287 (1962).
36. H.C. Bryant *et al.*, *Phys. Rev. Lett.* **38**, 228 (1977).
37. S. Inouye *et al.*, *Nature* **392**, 154 (1998).
38. Y. Kagan, E.L. Surkov, and G.V. Shlyapnikov, *Phys. Rev. Lett.* **79**, 2604 (1997).
39. P. Courteille, R.S. Freeland, and D.J. Heinzen, *Phys. Rev. Lett.* **81**, 69 (1998).
40. E.A. Cornell, private communication.
41. F.A. v. Abeelen and B.J. Verhaar, private communication.
42. F.A. v. Abeelen, B.J. Verhaar, and A.J. Moerdijk, *Phys. Rev. A* **55**, 4377 (1997).
43. T.-L. Ho and V.B. Shenoy, *Phys. Rev. Lett.* **77**, 3276 (1996).
44. T.-L. Ho, *Phys. Rev. Lett.* **81**, 742 (1998).
45. T. Ohmi and K. Machida, *J. Phys. Soc. Jpn.* **67** (1998), in press.
46. C.K. Law, H. Pu, and N.P. Bigelow, *Phys. Rev. Lett.*, submitted, cond-mat/9807258 (1998).
47. C.J. Myatt, E.A. Burt, R.W. Ghrist, E.A. Cornell, and C.E. Wieman, *Phys. Rev. Lett.* **78**, 586 (1997).
48. D.S. Hall, M.R. Matthews, J.R. Ensher, C.E. Wieman, and E.A. Cornell, *Phys. Rev. Lett.*, submitted, cond-mat/9804138 (1998).
49. D.S. Hall, M.R. Matthews, C.E. Wieman, and E.A. Cornell, *Phys. Rev. Lett.*, submitted, cond-mat/9805327 (1998).
50. E.D. Siggia and A.E. Ruckenstein, *Phys. Rev. Lett.* **44**, 1423 (1980).
51. E. Timmermans, submitted, cond-mat/9709301 (1997).
52. B.D. Esry, C.H. Greene, J.P. Burke, and J.L. Bohn, *Phys. Rev. Lett.* **78**, 3594 (1997).
53. P. Öhberg and S. Stenholm, *Phys. Rev. A* **57**,1272 (1998).
54. H. Pu and N.P. Bigelow, *Phys. Rev. Lett.* **80**,1130 (1998).
55. P. Ao and S.T. Chui, submitted, (1998).
56. T. Busch, J.I. Cirac, V.M. Pérez Garcia and P. Zoller, *Phys. Rev. A* **56**, 2978 (1997).
57. R. Graham and D. Walls, *Phys. Rev. A* **57**, 484 (1998).
58. H. Pu and N.P. Bigelow, *Phys. Rev. Lett.* **80**, 1134 (1998).
59. B.D. Esry and C.H. Greene, *Phys. Rev. A* **57**, 1265 (1998).
60. J. Stenger, S. Inouye, D.M. Stamper-Kurn, H.-J. Miesner, A.P. Chikkatur, and W. Ketterle, *Nature*, submitted.
61. K. Huang, *Statistical Mechanics* (Wiley, New York, ed. 2., 1987).
62. W.E. Lamb Jr. and A. Nordsieck, *Phys. Rev.* **59**, 677 (1941).
63. M.R. Andrews *et al.*, *Science* **273**, 84 (1996).
64. M.R. Andrews *et al.*, *Phys. Rev. Lett.* **79**, 553 (1997).
65. D.M. Stamper-Kurn *et al.*, *Phys. Rev. Lett.* **81**, 500 (1998).
66. F. Dalfovo, S. Giorgini, L.P. Pitaevskii, and S. Stringari, e-print cond-mat/9806038.
67. Yu. Kagan, E.L. Surkov, and G.V. Shlyapnikov, *Phys. Rev. A* **54**, R1753 (1996).
68. Yu. Kagan, E.L. Surkov, and G.V. Shlyapnikov, *Phys. Rev. A* **55**, R18 (1996).
69. Y. Castin and R. Dum, *Phys. Rev. Lett.* **77**, 5315 (1996).
70. F. Dalfovo *et al.*, *Phys. Rev. A* **56**, 3840 (1997).
71. F. Dalfovo, C. Minniti, and L.P. Pitaevski, *Phys. Rev. A* **56**, 4855 (1997).

Spin domains in ground state spinor Bose-Einstein condensates

J. Stenger, S. Inouye, D.M. Stamper-Kurn, H.-J. Miesner, A.P. Chikkatur, and W. Ketterle

Department of Physics and Research Laboratory of Electronics,
Massachusetts Institute of Technology, Cambridge, MA 02139

Bose Einstein condensates of dilute atomic gases, characterized by a macroscopic population of the quantum mechanical ground state, are a new, weakly interacting quantum fluid[1, 2, 3]. In most experiments condensates in a single weak field seeking state are magnetically trapped. These condensates can be described by a scalar order parameter similar to the spinless superfluid ^{4}He. Even though alkali atoms have angular momentum, the spin orientation is not a degree of freedom because spin flips lead to untrapped states and are therefore a loss process. In contrast, the recently realized optical trap for sodium condensates[4] confines atoms independently of their spin orientation. This opens the possibility to study spinor condensates which represent a system with a vector order parameter instead of a scalar. Here we report a study of the equilibrium state of spinor condensates in an optical trap. The freedom of spin orientation leads to the formation of spin domains in an external magnetic field. The structure of these domains are illustrated in spin domain diagrams. Combinations of both miscible and immiscible spin components were realized.

A variety of new phenomena is predicted[5, 6, 7] for spinor condensates, such as spin textures, propagation of spin waves and coupling between superfluid flow and atomic spin. To date such effects could only be studied in superfluid ^{3}He, which can be described by Bose Einstein condensation of Cooper pairs of quasi particles having both spin and orbital angular momentum[8]. Compared to the strongly interacting ^{3}He, the properties of weakly interacting Bose Einstein condensates of alkali gases can be calculated by mean field theories in a much more straightforward and simple way.

Other systems which go beyond the description with a single scalar order parameter are condensates of two different hyperfine states of ^{87}Rb confined in magnetic traps. Recent experimental studies have explored the spatial separation of the two components[9, 10] and their relative phase[11]. Several theoretical papers describe their structure[12, 13, 14, 15, 16, 17, 18] and their collective excitations[19, 20, 21, 22].

Compared to these two component condensates, spinor condensates have several new features including the vector character of the order parameter and the changed role of spin relaxation collisions which allow for population exchange among hyperfine states without trap loss. In contrast, for ^{87}Rb experiments trap loss due to spin relaxation severely limits the lifetime.

We consider an $F=1$ spinor condensate subject to spin relaxation, in which two $m_F=0$ atoms can collide and produce an $m_F=+1$ and an $m_F=-1$ atom and vice versa. We investigate the distribution of hyperfine states and the spatial distribution in equilibrium assuming conservation of the total spin.

The ground state spinor wave function is found by minimizing the free energy[5]

$$K = \int d^3r\, n \left[V + \frac{c_0 n}{2} + \frac{c_2 n}{2} \langle \vec{F} \rangle^2 + E_{ze} - p_0 \langle F_z \rangle \right], \qquad (1)$$

where kinetic energy terms are neglected in the Thomas-Fermi approximation which is valid as long as the dimension of spin domains (typically 50 μm) is larger then the penetration depth[18] (typically 1 μm). V is the trapping potential, n is the density, $\vec{F}$ is the angular momentum per atom, and E_{ze} is the Zeeman energy in an external magnetic field. The Lagrange multiplier p_0 accounts for the total spin conservation. The mean field energy in Eqn. (1) consists of a spin independent part proportional to c_0 and a spin dependent part proportional to $c_2\langle \vec{F} \rangle^2$. The coefficients c_0 and c_2 are related to the scattering lengths a_0 and a_2 for two colliding atoms with total angular momentum $F_{tot} = 0$ or $F_{tot} = 2$ by $c_0 = 4\pi\hbar^2\bar{a}/M$ and $c_2 = 4\pi\hbar^2\Delta a/M$ with $\bar{a} = (2a_2 + a_0)/3$, $\Delta a = (a_2 - a_0)/3$, and M for the atomic mass[5]. The spin dependent interaction originates from the term $c_2\vec{F}_1 \cdot \vec{F}_2$ in the interaction of two atoms, which is ferromagnetic for $c_2 < 0$ and anti-ferromagnetic for $c_2 > 0$.

In the Bogoliubov approach the many body ground state wave function is represented by the spinor wave function

$$\Psi(\vec{r}) = \sqrt{n(\vec{r})}\,\zeta(\vec{r}) = \sqrt{n(\vec{r})}\,(\zeta_+(\vec{r}), \zeta_0(\vec{r}), \zeta_-(\vec{r}))\,, \tag{2}$$

where $\zeta_+, \zeta_0, \zeta_-$ denote the amplitudes for the $m_F = +1, 0, -1$ states, respectively, and $|\zeta|^2 = 1$.

The Zeeman energy E_{ze} is given by

$$E_{ze} = E_+|\zeta_+|^2 + E_0|\zeta_0|^2 + E_-|\zeta_-|^2 = E_0 - \tilde{p}\langle F_z\rangle + q\langle F_z^2\rangle. \tag{3}$$

E_+, E_0, E_- are the Zeeman energies of the $m_F = +1, 0, -1$ states, $2q \equiv E_+ + E_- - 2E_0$ is the Zeeman energy difference in a spinflip collision, and $2\tilde{p} \equiv E_- - E_+$. The E_0 term can be included in the trapping potential V. The parameter $\tilde{p}$ can be combined with the Lagrange multiplier p_0 to give $p \equiv \tilde{p} + p_0$.

In the following we determine the spinor which minimizes the spin-dependent part K_s of the free energy:

$$K_s = c\langle\vec{F}\rangle^2 - p\langle F_z\rangle + q\langle F_z^2\rangle, \tag{4}$$

where $c = c_2 n/2$. The minimization of Eqn. (4) for different values of the parameters c, p, and q is straightforward, and is shown graphically in the form of spin-domain diagrams in Fig. 1.

Experimentally, the values of c, p, and q can be varied arbitrarily, representing any region of the spin domain diagram. The magnitude (but not the sign) of the coefficient c is varied by changing the density n, either by changing the trapping potential, or by studying condensates with different numbers of atoms. In this study, the axial length of the trapped condensate is more than 60 times larger than its radial size, and thus we consider the system one dimensional, and integrate over the radial coordinates, obtaining $n = 2n_0/3$ where n_0 is the density at the radial center. This integration assumes a parabolic density profile within the Thomas Fermi approximation. The value of q can be changed by applying a weak external bias field B_0: q then corresponds to the quadratic Zeeman shift $q = \hat{q}B_0^2$. The coefficient p arises both from the linear Zeeman shift and from the Lagrange multiplier p_0 which is determined by the total spin of the system. For a system with zero total spin in a homogenous bias field B_0, p_0 cancels the linear Zeeman shift due to B_0, yielding $p = 0$. Positive (negative) values of p are achieved for condensates with a positive (negative) overall spin. Finally, the coefficients can be made to vary spatially across the condensate. In particular, applying a field gradient B' along the axis of the trapped condensate causes p to vary along the condensate length. For a condensate with zero total spin, $p = \mu B' z$ where z is the axial coordinate with $z = 0$ at the center of the condensate. Thus, the condensate samples a vertical line in the spin domain diagrams of Fig. 1. The center of this line lies at $p = 0$, and its length is given by the condensate length scaled by $\mu B'$.

The experimental study of spinor condensates required techniques to selectively prepare and probe condensates in arbitrary hyperfine states. Spinor condensates were prepared in several steps. Laser cooling and evaporative cooling were used to produce sodium condensates in the $m_F = -1$ state in a cloverleaf magnetic trap[23]. The condensates were then transfered into an optical dipole trap consisting of a single focused infrared laser beam[4]. Arbitrary populations of the three hyperfine states were prepared using rf transitions[4]. After the spin preparation, a bias field B_0 and a field gradient B' were applied for a variable amount of time (as long as 30 s), during which the atoms relaxed towards their equilibrium distribution, as shown in fig. 2.

The profiles in Fig. 3 were obtained from vertical cuts through absorption images. They provide clear evidence of anti ferromagnetic interaction. The spin structure is consistent with the corresponding spin domain diagram in fig. 1 **a**. Overlapping $m_F = \pm 1$ clouds as observed are incompatible with the assumption of ferromagnetic interaction.

The strength $c = (50 \pm 20)$ Hz of the anti-ferromagnetic interaction was estimated by determining z_b, the location of the $m_F = 0$ to the $m_F = \pm 1$ boundary, and by plotting $p = \mu B' z_b$ versus the quadratic Zeeman shift $q = \hat{q}B_0^2$ as shown in Fig. 4. With $n = (2.9 \pm 0.5) \times 10^{14}\,\mathrm{cm}^{-3}$ the difference between the scattering lengths can be determined to $a_2 - a_0 = 3\Delta a = (3.5 \pm 1.5)a_B = (0.19 \pm 0.08)\,\mathrm{nm}$ where a_B denotes the Bohr radius. This result is in rough agreement with a theoretical calculation of $a_2 - a_0 = (5.5 \pm 0.5)a_B$[24]. The anti ferromagnetic interaction energy corresponds to 2.5 nK in

our condensates. Still, the magnetostatic (ferromagnetic) interaction between the atomic magnetic moments is about ten times weaker. It is interesting to note that the optically trapped samples in which the domains were observed were at a temperature of the order of 100 nK, far larger than the anti ferromagnetic energy. The formation of spin domains occurs only in a Bose Einstein condensate.

Fig. 3 c shows a profile of the density distribution for a cloud at $B_0 = 20\,\mathrm{mG}$ and almost canceled gradient ($B' < 2\,\mathrm{mG/cm}$). No $m_F = 0$ region can be identified. The cloud was prepared with a small total angular momentum. Due to the almost zero gradient and the non zero angular momentum the cloud corresponds to a point in the shaded region in Fig. 1 a, rather than a vertical line with no offset as discussed before with finite gradients and zero angular momentum. The different widths of the profiles are probably caused by residual field inhomogenities. Fig. 3 c demonstrates the complete miscibility of the $m_F = \pm 1$ components.

For a homogenous two component system the criterion for miscibility (immiscibility) is $a_{ab} < (>)\sqrt{a_a a_b}$[14, 15, 18], when the mean field energy is parametrized as $(2\pi\hbar^2/M)(n_a^2 a_a + n_b^2 a_b + 2n_a n_b a_{ab})$. Here, $n_{a,b}$ and $a_{a,b}$ are densities and scattering lengths for the components a and b, and the scattering length a_{ab} characterizes the interactions between particles a and b. In our spinor condensate with mixtures of the $m_F \pm 1$ components, we have $a_{-1} = a_{+1} = \bar{a} + \Delta a$ and $a_{-1+1} = \bar{a} - \Delta a$. Thus $\Delta a > 0$, like experimentally observed, implies miscibility. For a mixture of the $m_F = 1$ and $m_F = 0$ components, we find $a_0 = \bar{a}$, $a_{+1} = \bar{a} + \Delta a$ and $a_{0+1} = \bar{a} + \Delta a$, corresponding to immiscibility. For the ^{87}Rb experiments[9, 10] it is not clear whether the two components are miscible or overlap only in a surface region due to kinetic energy[25].

In conclusion, Bose Einstein condensates of sodium occupying all three hyperfine states of the $F = 1$ ground state multiplet were optically trapped in low magnetic fields. The hyperfine states are coupled by spin exchange processes, resulting in the formation of spin domains. We developed spin domain diagrams for both the anti ferromagnetic and the ferromagnetic case, and showed that sodium has anti ferromagnetic interactions, whereas the opposite case is predicted for the ^{87}Rb $F = 1$ spin multiplet[24]. All regions in the spin domain diagrams are accessible with our experimental technique and thus any combination of the three hyperfine components can be realized by applying small external magnetic fields. Of special interest for future work is the zero magnetic field case, where the rotational symmetry should be spontaneously broken. We observed both miscibility and immiscibility of hyperfine components. Thus the dynamics and possible metastable configurations[7] of two interpenetrating, miscible superfluid components ($m_F = \pm 1$) with arbitrary admixtures of an immiscible component ($m_F = 0$) can now be studied.

References

[1] Anderson, M. H., Ensher, J. R., Matthews, M. R., Wieman, C. E., & Cornell, E. A. Observation of Bose-Einstein condensation in a dilute atomic vapor. *Science*, **269**, 198 201 (1995).

[2] Davis, K. B., et al. Bose-Einstein condensation in a gas of sodium atoms. *Phys. Rev. Lett.*, **75**, 3969 3973 (1995).

[3] Bradley, C. C., Sackett, C. A., & Hulet, R. G. Bose-Einstein condensation of lithium: Obervation of limited condensate number. *Phys. Rev. Lett.*, **78**, 985 989 (1997).

[4] Stamper-Kurn, D. M., et al. Optical confinement of a Bose-Einstein condensate. *Phys. Rev. Lett.* **80**, 2027 2030 (1998).

[5] Ho, T.-L. Spinor Bose condensates in optical traps. *Phys. Rev. Lett.* **81**, 742 745 (1998).

[6] Ohmi, T. & Machida, K. Bose Einstein condensation with internal degrees of freedom in alkali atom gases. *J. Phys. Soc. Jpn.* **67** (1998), in the press.

[7] Law, C.K., Pu, H., & Bigelow, N.P. Quantum spins mixing in spinor Bose Einstein condensates. *Phys. Rev. Lett.*, submitted, cond-mat/9807258 (1998).

[8] Vollhardt, D. & Wölfle, P. The superfluid phases of ^{3}He. *Taylor Francis, London* (1990).

[9] Myatt, C.J., Burt, E.A., Ghrist, R.W., Cornell, E.A., & Wieman, C.E. Production of two overlapping Bose Einstein condensates by sympathetic cooling. *Phys. Rev. Lett.* **78**, 586 589 (1997).

[10] Hall, D.S., Matthews, M.R., Ensher, J.R., Wieman, C.E., & Cornell, E.A. The dynamics of component separation in a binary mixture of Bose Einstein condensates. *Phys. Rev. Lett.*, submitted, cond-mat/9804138 (1998).

[11] Hall, D.S., Matthews, M.R., Wieman, C.E., & Cornell, E.A., Measurements of relative phase in binary mixtures of Bose Einstein condensates. *Phys. Rev. Lett.*, submitted, cond-mat/9805327 (1998).

[12] Siggia, E.D. & Ruckenstein, A.E. Bose Condensation in spin polarized atomic hydrogen. *Phys. Rev. Lett.* **44**, 1423 1426 (1980).

[13] Ho, T.-L. and Shenoy, V.B. Binary mixtures of Bose condensates of alkali atoms. *Phys. Rev. Lett.* **77**, 3276 3279 (1996).

[14] Timmermans, E. Phase separation in Bose Einstein condensates. Submitted, cond-mat/9709301

[15] Esry, B.D., Greene, C.H., Burke, J.P., and Bohn, J.L. Hartree Fock theory for double condensates. *Phys. Rev. Lett.* **78**, 3594 3597 (1997).

[16] Öhberg, P. & Stenholm, S. Hartree Fock treatment of the two component Bose Einstein condensate. *Phys. Rev.* **A57**, 1272 1279 (1998).

[17] Pu, H. & Bigelow, N.P. Properties of two species Bose condensates. *Phys. Rev. Lett.* **80**, 1130 1133 (1998).

[18] Ao, P. & Chui, S.T. Binary Bose Einstein condensate mixtures in weakly and strongly segregated phases. Submitted, (1998).

[19] Busch, T., Cirac, J.I., Pérez García, V.M., & Zoller, P. Stability and collective excitations of a two component Bose Einstein condensed gas: a moment approach. *Phys. Rev.* **A56**, 2978 2983 (1997).

[20] Graham, R. & Walls, D. Collecitve excitations of trapped binary mixtures of Bose Einstein condensed gases. *Phys. Rev.* **A57**, 484 487 (1998).

[21] Pu, H. and Bigelow,N.P. Collective excitations, metastability, and nonlinear response of a trapped two species Bose Einstein condensate. *Phys. Rev. Lett.* **80**, 1134 1137 (1998).

[22] Esry, B.D. & Greene, C.H. Low lying excitations of double Bose Einstein condensates. *Phys. Rev.* **A57**, 1265 1271 (1998).

[23] Mewes, M.-O., et al. Bose-Einstein condensation in a tightly confining dc magnetic trap. *Phys. Rev. Lett.* **77**, 416 419, (1996).

[24] Burke, J.P., Greene, C.H., & Bohn, J.L. Multichannel cold collisions: simple dependencies on energy and magnetic field. *Phys. Rev. Lett.*, submitted.

[25] Cornell, E.A. private communication.

We acknowledge stimulating discussions with Jason Ho and Chris Greene. This work was supported by the Office of Naval Research, NSF, Joint Services Electronics Program (ARO), NASA, and the David and Lucile Packard Foundation. J.S. would like to acknowledge support from the Alexander von Humboldt-Foundation, D.M.S.-K. from the JSEP Graduate Fellowship Program, and A.P.C. from the NSF.

Figure captions:

Figure 1: Spin domain diagrams for spin one condensates. The structure of the ground state spinor is shown as a function of the linear ($\sim p$) and quadratic ($\sim q$) Zeeman energies. Hyperfine components are mixed inside the shaded regions. Solid lines indicate a discontinuous change of state populations whereas dashed lines indicate a gradual change. The behaviour for $q < 0$ is also shown although it is not relevant for this experiment. For $c = 0$, the Zeeman energy causes the cloud to separate into three domains with $m_F = +1, 0, -1$ and with boundaries at $|p| = q$, as shown in **b**. For $c_2 \neq 0$, the mean field energy shifts the boundary region between domains and leads to regions of overlapping spin components. In the anti ferromagnetic case (**a**), the $m_F = 0$ component and the $m_F = \pm 1$ components are immiscible (including the kinetic energy terms in Eqn. (1) would lead to a thin boundary layer) and the boundary occurs at $|p| = q + c$. For small bias fields, with $q < c$ and $|p| < 2c$, the $m_F = 0$ domain is bordered by domains in which $m_F = \pm 1$ components are mixed. The ratio of the $m_F = \pm 1$ populations in these regions does not depend on q, but is given by $|\zeta_+|^2/|\zeta_-|^2 = (2c + p)/(2c - p)$. In this region of small fields, the boundary to the $m_F = 0$ component lies at $|p| = 2\sqrt{cq}$. In the ferromagnetic case (**c**) all three components are generally miscible, and have no sharp boundaries. Pure $m_F = 0$ domains occur for $|p| \leq \sqrt{q(q - 4|c|)}$ and pure $m_F = \pm 1$ domains for $|p| > q$. Here, in contrast to the anti ferromagnetic case, a pure $m_F = 0$ condensate is skirted by regions where it is mixed predominantly with either the $m_F = -1$ or the $m_F = +1$ component. The contribution of the third component is very small ($< 2\%$). In all mixed regions the $m_F = 0$ component is never the least populated of the three spin components. This qualitative feature can be used to rule out that $F = 1$ sodium atoms have ferromagnetic interactions.

Figure 2: Formation of ground state spin domains. Absorption images of ballistically expanding spinor condensates show both the spatial and hyperfine distributions. Arbitrary populations of the three hyperfine states were prepared using rf transitions (Landau Zener sweeps) [4]. At a bias field of about 40 G the transitions from $m_F = -1$ to $m_F = 0$ and from $m_F = 0$ to $m_F = +1$ differ in frequency by about 0.9 MHz due to the quadratic Zeeman shift and they could be driven separately. The images of clouds with various dwell times in the trap show the evolution to the same equilibrium for condensates prepared in either a pure $m_F = 0$ state (upper row) or in equally populated $m_F = \pm 1$ states (lower row). Between 5 s to 15 s dwell time, the distribution did not significantly change, although the density decreased due to three body recombination. The bias field during the dwell time was $B_0 = 20$ mG and the field gradient was $B' = 11$ mG/cm. These images were taken after the optical trap was suddenly switched off and the atoms were allowed to expand. Due to the large aspect ratio (typically 60), the expansion was almost purely in the radial directions. All the mean field energy was released after less than 1 ms, after which the atoms expanded as free particles. Thus, a magnetic field gradient, which was applied after 5 ms time of flight to yield a Stern Gerlach separation of the cloud, merely translated the three spin components without affecting their shapes. In this manner, the single time of flight images provided both a spatial and spin state description of the trapped cloud. Indeed, the shapes of the three clouds fit together to form a smooth total density distribution. After a total time of flight of 25 ms the atoms were optically pumped into the $F = 2$ hyperfine state and observed using the $m_F = +2$ to $m_F = +3$ cycling transition. This technique assured the same transition strength for atoms originating from different spin states. The size of the field of view for a single spinor condensate is 1.7 mm × 2.7 mm.

Figure 3: Miscible and immiscible spin domains. Axial column density profiles of spinor Bose-Einstein condensates are shown, obtained from time-of-flight absorption images as in Fig. 2. The profiles of the $m_F = \pm 1$ components were shifted to undo the Stern-Gerlach separation. At low bias fields (Fig. 3 **a**), the $m_F = 0$ component was skirted on both sides by $m_F = \pm 1$ components with significant $m_F = \mp 1$ admixtures thus demonstrating the anti ferromagnetic interaction (also visible in Fig. 2). At higher fields (Fig. 3 **b**), the $m_F = \pm 1$ components are pushed apart further by a larger $m_F = 0$ component and the $m_F = \mp 1$ admixtures vanish. They could not be resolved for quadratic Zeeman energies $q > 20\,\mathrm{Hz}$. The anti ferromagnetic interaction leads to immiscibility of the $m_F = 0$ and the $m_F = \pm 1$ components. The kinetic energy in this boundary region, which is small compared to the total mean field energy, is released in the axial direction. Due to this axial expansion of the cloud in the time of flight and due to imperfections in the imaging system including the limited pixel resolution, the $m_F = 0$ to $m_F = \pm 1$ boundary is not sharp. Fig. 3 **c** demonstrates the complete miscibility of the $m_F = \pm 1$ components. The magnetic field parameters were $B_0 = 20\,\mathrm{mG}$, $B' = 11\,\mathrm{mG/cm}$ in **a**, $B_0 = 100\,\mathrm{mG}$, $B' = 11\,\mathrm{mG/cm}$ in **b**, and $B_0 = 20\,\mathrm{mG}$, $B' < 2\,\mathrm{mG/cm}$ in **c**.

Figure 4: Estimate of the anti ferromagnetic interaction energy c. Plotted is the linear Zeeman energy $p = |\mu B' z_b|$ at the boundary between the $m_F = 0$ and $m_F = \pm 1$ regions versus the quadratic Zeeman shift $q = \dot{q} B_0^2$. $\dot{q} = g_s^2 \mu_B^2 / 16 h^2 \nu_{hfs} = 278\,\mathrm{Hz/G^2}$, and $\mu = g_s \mu_B / 4h = 700\,\mathrm{kHz/G}$. g_s denotes the electron g factor. ν_{hfs} the hyperfine splitting frequency, and μ_B the Bohr magneton. The solid line is a fit of the function $|p| = 2\sqrt{qc}$ for $q < c$ and $|p| = q + c$ for $q > c$. Extrapolating the linear part to zero bias field (dashed line) yields $c = (50 \pm 20)\,\mathrm{Hz}$. The data points at a given bias field represent $p = \mu B' z_b$ for different gradient fields B' and thus $m_F = 0$ regions of different size. The scatter of these points is mainly due to a residual magnetic field inhomogenities, resulting in small deviations of the local gradient B'. The error bar represents the relative error of all data points of 30 % in p and 5 % in q as estimated from the uncertainties in the magnetic field calibration. Furthermore the limited pixel resolution and contributions of the kinetic energy in the condensate to the axial expansion enhance the errors for the determination of z_b of small $m_F = 0$ regions.

Figures:

Figure 1:

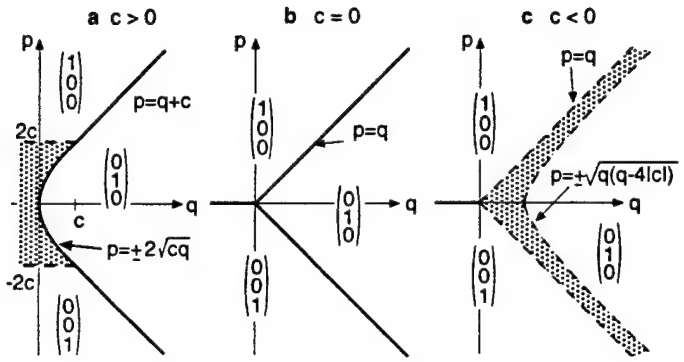

Figure 2:

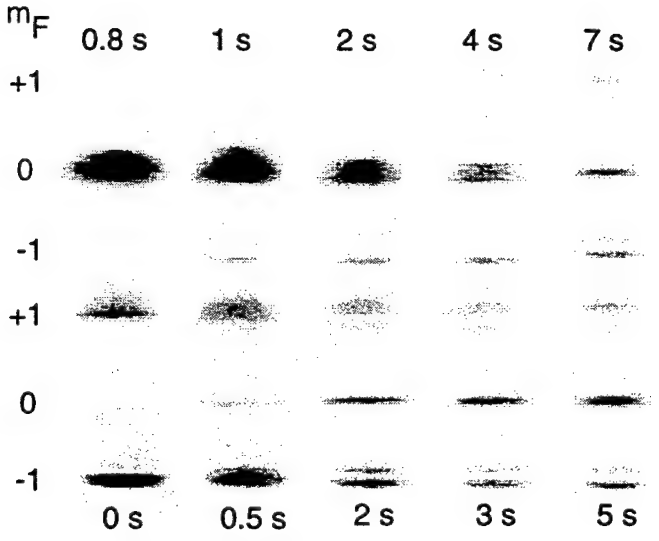

Figure 3:

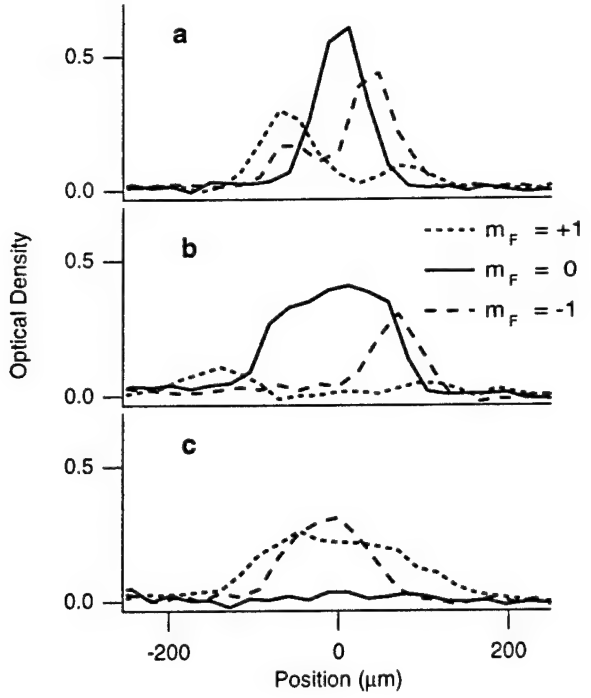

Figure 4:

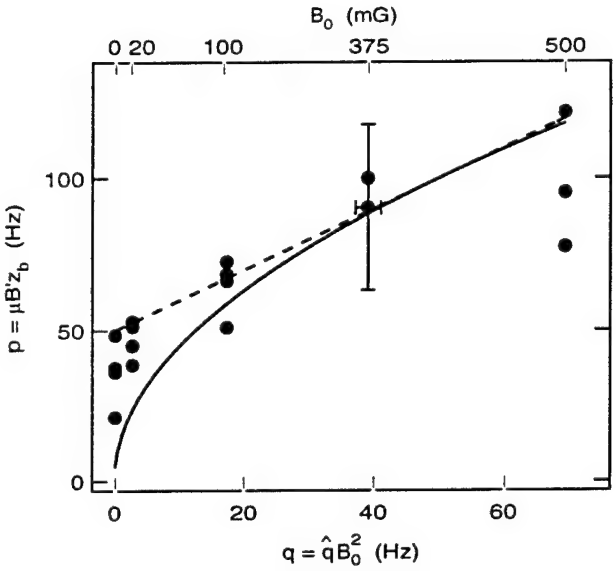

Reversible Formation of a Bose-Einstein Condensate

D.M. Stamper-Kurn, H.-J. Miesner, A.P. Chikkatur, S. Inouye, J. Stenger, and W. Ketterle
Department of Physics and Research Laboratory of Electronics,
Massachusetts Institute of Technology, Cambridge, MA 02139
()

We present a method of adiabatically changing the local phase-space density of an ultracold gas, using a combination of magnetic and optical forces. Applying this method, we observe phase-space density increases in a gas of sodium atoms by as much as 50-fold. The transition to Bose-Einstein condensation was crossed reversibly, attaining condensate fractions of up to 30%. Measurements of the condensate fraction reveal its reduction due to interactions.

The physical properties of atomic gases change dramatically when quantum degeneracy is reached, i.e. when the ground state population approaches unity [1]. Recent successes in reaching quantum degeneracy with Bose gases [2–4] have relied on non-adiabatic, irreversible methods such as laser and evaporative cooling. The possibility of changing the ground state population by an adiabatic (i.e. isentropic) change in the trapping potential had been overlooked for quite some time [5]. Indeed, in the case of an ideal gas, adiabatic changes in the *strength* of the trapping potential do not change the ground state population [6,7]. However, Pinkse and collaborators [8] recently showed, both theoretically and experimentally, that by changing the *form* of the trapping potential, the population in the ground state can be changed without changing the entropy. For a non-degenerate gas the ground state population is identical to the phase-space density $\Gamma = n\lambda_T^3$, where n is the density of the gas and λ_T is the thermal de Broglie wavelength. Within the type of trap deformations considered in Ref. [8] the maximum increase of phase-space density is limited to a factor of 20.

In this Letter, we show that a more general deformation of the trapping potential can increase the phase-space density by an arbitrary factor, and implement this scheme using a combination of magnetic and optical forces. Furthermore, we demonstrate the ability to cross the Bose-Einstein condensation (BEC) phase transition reversibly.

Adiabatic increase in phase-space density. The type of trap deformations which we study can be understood with the following "two-box" model. Consider a classical gas of N atoms confined in a box of volume $V_0 = V_1 + V_2$ with an initial phase-space density Γ_0. Suppose that the potential within a sub-volume V_2 of the box is lowered to a final well-depth U. In this final potential, the gas equilibrates at a temperature T_f, and the density in V_2 will be higher than that in V_1 by the Boltzmann factor $e^{U/k_B T_f}$. Using the condition of constant entropy and constant particle number, one obtains the relative increase of phase-space density in V_2 compared to that in V_0 before compression:

$$\ln\left(\Gamma_2/\Gamma_0\right) = \frac{U/k_B T_f}{1 + (V_2/V_1)e^{U/k_B T_f}} \,. \qquad (1)$$

For deep potential wells, where $U/k_B T_f \gg \ln(V_1/V_2)$, there is no increase in phase-space density since all of the gas becomes confined in V_2, and the adiabatic deformation corresponds simply to a uniform compression of the gas. For shallow potential wells ($U/k_B T_f \ll \ln(V_1/V_2)$), the phase-space density in V_2 increases as $e^{U/k_B T_f}$. As U is varied between these limits, the phase-space density increase reaches a maximum which is greater than $(V_1/V_2)^{1/2}$. Thus, by choosing an extreme ratio of volumes V_1/V_2, an arbitrarily large increase in phase-space density Γ_2/Γ_0 is possible.

To demonstrate this phase-space density increase in a gas of trapped atoms, a narrow potential well (analogous to V_2) was added to a broad harmonic potential (corresponding to V_1) by focusing a single infrared laser beam at the center of a magnetic trap. First a gas of atomic sodium was evaporatively cooled to a temperature higher than the BEC phase transition temperature in the cloverleaf magnetic trap [9]. The number of atoms and their temperature were adjusted by varying the final radio frequency (rf) used in the rf-evaporative cooling stage [10]. Afterwards, the magnetically trapped cloud was decompressed by slowly reducing the currents in the magnetic trapping coils. Time-of-flight absorption imaging was used to characterize the cloud. The total number of atoms N was determined by integrating the column density across the cloud, and the initial temperature T_0 was determined by one-dimensional Gaussian fits to the wings of the density distribution. From these, we determined the fugacity z of the gas by the relation $g_3(z) = N(\hbar\bar{\omega}/k_B T_0)^3$, and then its phase-space density by $\Gamma_0 = g_{3/2}(z)$, where $g_n(z) = \sum_{i=1}^{\infty} z^i/i^n$ [11]. Here, $\bar{\omega}$ is the geometric-mean trapping frequency of the magnetic trap, as determined by *in situ* measurements [12]. These phase-space density measurements were calibrated with images from magnetically trapped clouds at the phase transition.

The optical setup was similar to that used in Ref. [13]. The infrared laser power was gradually ramped-up from zero to a power P_c at which the onset of BEC was seen

in time-of-flight images of clouds released from the deformed trap; this implied $\Gamma_f = g_{3/2}(1) = 2.612$ for the final phase-space density. These time-of-flight images allowed us to determine the final temperature T_f. The depth of the optical potential well was given by $U_c/k_B = 37\mu\text{K}\ P_c/w_0^2$ (μm^2/mW), where w_0 is the $1/e^2$ beam-waist radius at the focus. The ramp-up time was made long enough to ensure that the trap deformation was adiabatic, but also short enough to minimize heating and trap loss. Ramp-up times of up to 10 s were used.

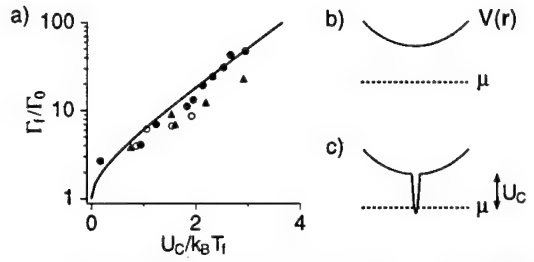

FIG. 1. Phase-space density increase to reach BEC vs. normalized well-depth (a). Various trap settings were used: $\bar{\omega} = 2\pi \times 100$ Hz, $w_0 = 9\,\mu$m (triangles); $\bar{\omega} = 2\pi \times 100$ Hz, $w_0 = 18\,\mu$m (open circles); and $\bar{\omega} = 2\pi \times 33$ Hz, $w_0 = 18\,\mu$m (closed circles). The solid line gives the prediction of Eq. (3). (b) Prior to deformation, the harmonic trapping potential $V(r)$ holds a cloud above the BEC transition temperature ($\mu < 0$). (c) When a potential well with depth $U_c = -\mu$ is added, a small condensate forms.

Fig. 1a shows the increases in phase-space density which were measured at three different settings of the trap parameters. A maximum increase by a factor of 50 was obtained. Condensates were observed in clouds with temperatures as high as 5 μK. Further increases were hindered by limitations in laser power and by limits to the ramp-up time set by the various heating and loss processes in the deformed trap. The scatter in the data is primarily due to statistical errors at the level of 30% in our measurements of U_c/k_BT_f, and in the determination of the transition point.

The well-depth U_c required to reach BEC can be understood by a simple model depicted in Fig. 1. We begin with a harmonically trapped gas with a chemical potential $\mu < 0$ (Fig. 1b). Then, by lowering a potential well to a depth U_c at which BEC occurs, one essentially measures μ as $\mu = -U_c$ (Fig. 1c). However, this simple picture neglects the change in the chemical potential and the temperature of the gas during the adiabatic compression. Thus, let us consider instead the condition of constant entropy. The entropy per non-condensed particle in a harmonically confined Bose gas is determined uniquely by its fugacity z [8]:

$$\frac{S}{N}(z) = 4\frac{g_4(z)}{g_3(z)} - \ln z \quad . \tag{2}$$

This equation describes the entropy of the gas before compression, with the fugacity given by z_0. After compression, because of the small volume of the potential well, the entropy per particle is approximately that of a harmonically trapped gas (Eq. (2)) with fugacity $z_f = e^{-U_c/k_BT_f}$ [15]. Here T_f is the final temperature of the gas. Constant entropy then implies $z_0 = z_f$. The initial phase-space density of the gas is $\Gamma_0 = g_{3/2}(z_0)$ and its final phase-space density is $\Gamma_f = g_{3/2}(1)$. Thus we obtain

$$\frac{\Gamma_f}{\Gamma_0} = \frac{g_{3/2}(1)}{g_{3/2}(\exp(-U_c/k_BT_f))} \quad . \tag{3}$$

This prediction, shown in Fig. 1a, describes our data well, and accounts for the universal behaviour of our measurements over a wide range of temperatures and well-depths.

One may also consider the process of adiabatically increasing the phase-space density as a change in the density of states $D(\epsilon)$ of the system. By increasing the well-depth in a small region of the trap, we lowered only the energy of the ground state and a few excited states. Thus Γ, a local quantity, increases as the ground state energy is brought closer to the chemical potential, while the entropy, a global property of the gas, is unchanged by the minimal modification of $D(\epsilon)$.

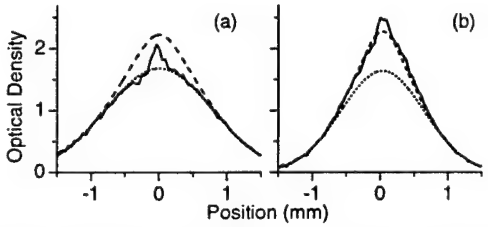

FIG. 2. Momentum distributions of the thermal cloud at the BEC phase transition show no Bose-enhancement for the deformed trap (a), but a clear Bose-enhancement for the purely magnetic trap (b). Both distributions show a small condensate peak. Lines show a Maxwell-Boltzmann distribution (dotted) and a Bose-Einstein distribution (for $z = 1$) (dashed) for clouds in a harmonic trap, which were fit to the thermal wings. The momentum distribution is shown as a profile across absorption images taken after 40 ms of ballistic expansion.

The fact that global properties of the gas are not affected by the trap deformation can also be seen in the momentum distributions probed by time-of-flight imaging [9,16]. The onset of BEC in the combined optical and magnetic trap is signaled only by the formation of a condensate peak. The remaining thermal cloud is well fit by a Maxwell-Boltzmann distribution, which describes a magnetically trapped cloud far from condensation (Fig. 2a). In contrast, at the BEC transition in the harmonic magnetic trap, the momentum distribution of the thermal cloud is clearly Bose-enhanced at low momenta (Fig. 2b).

Adiabatic condensation. We now turn to the studies of adiabatic, i.e., reversible, condensate formation. A cloud of about 50×10^6 atoms was cooled to the the transition temperature in the magnetic trap, at trap frequencies of $\omega_r = 2\pi \times 20\,\mathrm{Hz}$ and $\omega_z = 2\pi \times 13\,\mathrm{Hz}$ in the radial and axial direction, respectively. The power of the infrared laser beam (of radius $w_0 = 20\,\mu\mathrm{m}$), was ramped up over 1 s and held at a constant power for a dwell time of 1.5 s. Condensate fractions as small as 1% could be distinguished from the normal fraction by their anisotropic expansion in time-of-flight images [2,3]. The condensate number N_0 was determined by subtracting out the thermal cloud background using Gaussian fits to the thermal cloud in regions where the condensate was clearly absent.

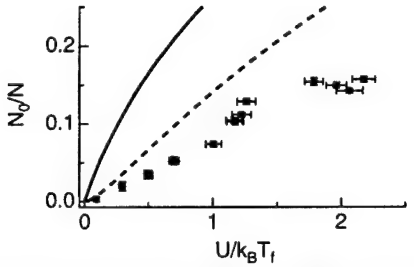

FIG. 3. Condensate formation by adiabatic trap deformation. The condensate fraction is plotted against the (normalized) well-depth. Lines show predictions for an ideal gas (solid) and for an interacting gas (dashed).

As shown in Fig. 3, the adiabatic trap deformation yielded condensate fractions of up to 15%; we observed condensate fractions of 30% with different trap settings. By varying the dwell time, we confirmed that clouds for which $U/k_BT_f < 1.5$ suffered no significant losses of condensate number due to three-body decay or heating, whereas those points with higher values of U/k_BT_f were affected by such losses.

For an ideal Bose gas, the result of this adiabatic change can be understood as follows. Before compression, the cloud of N particles at the BEC transition has an entropy S_i given by Eq. (2) as $S_i = N \times 4g_4(1)/g_3(1)$. After compression, the situation is similar to that indicated in Fig. 1c, i.e. because of the small volume of the attractive well, the cloud is well-described as a harmonically trapped gas with $\mu = -U$. Thus, accounting for the fact that condensate particles carry no entropy and again using Eq. (2), which gives the entropy per *non-condensed* particle, we equate the entropy before and after compression and obtain

$$\frac{N_0}{N} = 1 - \frac{4g_4(1)/g_3(1)}{4g_4(e^{-U/k_BT_f})/g_3(e^{-U/k_BT_f}) + U/k_BT_f}. \quad (4)$$

However, this simple prediction does not describe our findings well. The theory described above has two shortcomings. First, the approximation of using Eq. (2) for the deformed trap is not strictly valid. However, calculations which accounted for the true shape of the deformed potential changed the prediction of Eq. (4) only for $U/k_BT_f > 1$, and only slightly improved the fit to our data.

A second shortcoming is the neglect of interactions. It has been shown that the condensate fraction of harmonically trapped Bose gases with repulsive interactions is reduced in comparison to that of an ideal gas [17,18]. To estimate this effect in our system, we use the "semi-ideal" model of Ref. [18]. The thermal cloud is described as an ideal gas for which the chemical potential is raised by $gn_0 = 4\pi\hbar^2 a n_0/m$, where n_0 is the maximum condensate density, m the mass of sodium, and $a = 2.75$ nm its scattering length [19]. This simply corresponds to using Eq. (4) with the substitution $U \to U - gn_0$. We determined n_0 using the Gross-Pitaevskii equation in the Thomas-Fermi limit [20], and a harmonic approximation for the deformed trap potential at its center. Both approximations are valid for all data in Fig. 3.

This approach predicts a significant reduction of the condensate fraction (Fig. 3, dashed line), and the improved agreement with our data is strong evidence for this effect. In contrast to related studies in purely harmonic traps [9,16], which did not show evidence for interaction effects, this depletion is strongly enhanced by the shape of the deformed potential. The mean-field energy of the condensate gn_0 is large because the condensate forms in the tight optical potential, while the transition temperature T_c is small since it is determined by the weak magnetic potential. The remaining discrepancy between the "semi-ideal" prediction and our data may be due to our approximation to the entropy of the interacting gas, which fails for large values of gn_0/k_BT_f [21].

The reversibility of crossing the BEC phase transition was demonstrated by preparing a magnetically trapped cloud just above T_c. We then sinusoidally modulated the power of the infrared light at 1 Hz, between zero and 7 mW. This modulation frequency was significantly smaller than the magnetic trap frequencies ($\omega_r = 2\pi \times 48$ Hz and $\omega_z = 2\pi \times 16$ Hz). These low frequencies and a large optical focus ($w_0 = 18\,\mu$m) were used to minimize trap loss due to inelastic collisions.

During the first seven condensation cycles the condensate fraction oscillated between zero and 6% (Fig. 4); later probing showed repeated condensation for at least 15 cycles. The peak of these oscillations decreased slowly in time. The temperature oscillated with an amplitude of about 100 nK, while gradually rising by about 10 nK/s. This heating and the decrease of the peak condensate fraction are consistent with similar behaviour in clouds held at a constant infrared power [13]. Thus, within the stability limitations of our optical setup, the repeated crossing of the BEC phase transition appears fully adiabatic.

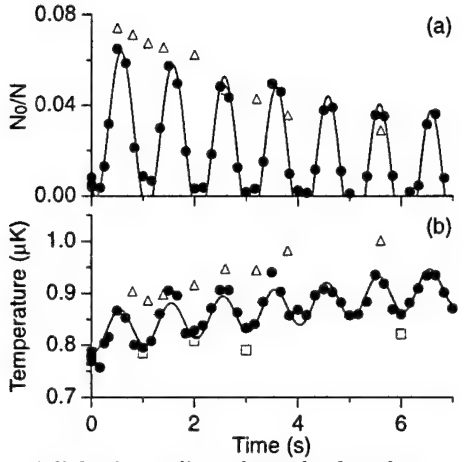

FIG. 4. Adiabatic cycling through the phase transition. Shown is the condensate fraction (a) and the temperature (b) vs time for the case of a modulated infrared beam (closed circles), an infrared beam ramped up to a constant power (open triangles), and no infrared light (open squares). The solid lines are guides to the eye.

This method of creating condensates provides insight into their formation, which was recently studied experimentally [22] and theoretically [23]. For example, in the experiment described above, the condensate fraction was found to lag about 70 ms behind the modulation of the laser power, which is a measure for the formation time. That this lag time is much shorter than the timescale for deforming the potential ($\approx$ 1 s) confirms that the repeated condensation is performed adiabatically.

In other experiments, by switching on the infrared light instantly, we observed condensation on time scales much faster than the oscillation periods in the magnetic trap and along the weakly confining axis of the optical trap. The resulting condensates showed striations in time-of-flight images, indicating that the condensates formed into excited states of the deformed potential. Such studies of shock-condensation might give new insight into the formation of quasi-condensates and condensation into excited states [24,25].

In conclusion we have demonstrated the adiabatic Bose-Einstein condensation of an ultracold gas of atomic sodium. Changes in the trapping potential resulted in large phase-space density increases and allowed for repeated crossings of the BEC phase transition. This method allows for detailed studies of condensate formation and the phase transition. The combined trapping potential widens the range of trap parameters over which BEC can be studied. This was used to strikingly enhance the role of interactions, and led to higher transition temperatures (up to 5 μK) than achieved in purely magnetic traps.

We thank Michael R. Andrews for discussions. This work was supported by the Office of Naval Research, NSF, Joint Services Electronics Program (ARO), NASA, and the David and Lucile Packard Foundation. A. P. C. acknowledges additional support from the NSF, D. M. S. -K. from JSEP, and J. S. from the Alexander von Humboldt-Foundation.

[1] A. Griffin, D.W. Snoke, and S. Stringari, *Bose-Einstein Condensation* (Cambridge University Press, Cambridge, 1995); Georgia Southern University BEC home page, http://amo.phy.gasou.edu/bec.html
[2] M.H. Anderson *et al.*, Science **269**, 198 (1995).
[3] K.B. Davis *et al.*, Phys. Rev. Lett. **75**, 3969 (1995).
[4] C.C. Bradley, C.A. Sackett, and R.G. Hulet, Phys. Rev. Lett. **78**, 985 (1997), see also: C.C.Bradley *et al.*, Phys. Rev. Lett. **75**, 1687 (1995).
[5] W. Ketterle and D.E. Pritchard, Phys. Rev. A **46**, 4051 (1992).
[6] F. Reif, *Fundamentals of Statistical and Thermal Physics* (McGraw-Hill Book Company, New York, 1965)
[7] For weakly interacting Bose gases this argument has to be modified; see: M. Houbiers, H.T.C Stoof, and E.A. Cornell, Phys. Rev. **A 56**, 2041 (1997).
[8] P. W. H. Pinkse *et al.*, Phys. Rev. Lett. **78**, 990 (1997).
[9] M.-O. Mewes *et al.*, Phys. Rev. Lett. **77**, 416 (1996).
[10] W. Ketterle and N.J. van Druten, in *Advances in Atomic, Molecular, and Optical Physics*, edited by B. Bederson and H. Walther (Academic Press, San Diego, 1996), Vol. 37, p 181.
[11] This assumes an ideal Bose gas and harmonic confinement; see: V. Bagnato, D. E. Pritchard, and D. Kleppner, Phys. Rev. **A 35**, 4354 (1987).
[12] D. M. Stamper-Kurn *et al.*, Phys. Rev. Lett. **81**, 500 (1998).
[13] D. M. Stamper-Kurn *et al.*, Phys. Rev. Lett. **80**, 2027 (1998).
[14] K. Huang, *Statistical Mechanics*, second edition (Wiley, New York, 1987).
[15] This approximation is valid for shallow potential wells ($U/k_BT \ll \ln(V_1/V_2)$), as discussed in the two-box model. Numerical calculations confirmed its validity for all data in Fig. 1a. Note that the effective volume of the magnetic trap (V_1) increases with temperature.
[16] J. R. Ensher *et al.*, Phys. Rev. Lett. **77**, 4984 (1996).
[17] V.V. Goldman, I.F. Silvera, and A.J. Leggett, Phys. Rev. B **24**,2870 (1981); R.J. Dodd, K. Burnett, M. Edwards, and C.W. Clark, Acta Physica Polonica **93**,45 (1998); S. Giorgini, L.P. Pitaevskii and S. Stringari, Phys. Rev. A **54**, R4633 (1996).
[18] M. Naraschewski and D.M. Stamper-Kurn, Phys. Rev. A (in press).
[19] E. Tiesinga *et al.*, J. Res. Natl. Inst. Stand. Technol. **101**, 505 (1996).
[20] G. Baym and C.J. Pethick, Phys. Rev. Lett **76**, 6 (1996).
[21] S. Giorgini, private communication.
[22] H.-J. Miesner *et al.*, Science **279**, 1005 (1998).
[23] C.W. Gardiner, P. Zoller, R.J. Ballagh, and M.J. Davis, Phys. Rev. Lett. **79**, 1793 (1997).

[24] Yu. Kagan, B.V. Svistunov, and G.V. Shlyapnikov, Sov. Phys. JETP **75**, 387 (1992).
[25] C.W. Gardiner *et al.*, preprint cond-mat/9801027 (unpublished).

Analytical description of a trapped semi-ideal Bose gas at finite temperature

M. Naraschewski
Jefferson Laboratory, Department of Physics, Harvard University, Cambridge, MA 02138, USA
ITAMP, Harvard-Smithsonian Center for Astrophysics, 60 Garden Street, Cambridge, MA 02138, USA

D.M. Stamper-Kurn
Department of Physics and Research Laboratory of Electronics, Massachusetts Institute of Technology, Cambridge, MA 02139
(17 March 1998)

Present experiments with Bose condensed gases can be largely described by a semi-ideal two-gas model. In this model, the condensate is influenced only by the mean-field repulsion among condensed atoms, while the thermal cloud is considered an ideal gas confined by an effective potential that consists of the external trap and the mean-field repulsion by the condensate. This simple, intuitive model provides explicit analytical expressions for the density distributions of the condensate and the thermal component. It describes the reduction of the condensate fraction relative to that of an ideal gas as a consequence of the positive chemical potential due to interactions in the condensate.

03.75.Fi,05.30.Jp

Recent experiments with Bose-Einstein condensed alkali gases (cf. e.g. [1, 2]) have been successfully described by different approximation schemes. The diluteness of these gases, expressed as $na^3 \ll 1$ where a is the two-body scattering length, allows a description in terms of an effective mean-field theory. At zero temperature the condensate can be described by the Gross-Pitaevskii equation [3, 4], a nonlinear Schrödinger equation. In present experiments interactions are strong enough so that the chemical potential μ is much larger than the level spacings $\hbar\omega_x$, $\hbar\omega_y$, and $\hbar\omega_z$ of the external harmonic potential. Therefore the use of the Thomas-Fermi approximation [5, 6], which neglects the kinetic energy of the condensate, has lead to a tremendous simplification in the understanding of these experiments.

Recently, much theoretical and experimental attention has been focused on finite temperature properties of Bose-condensed gases. A semiclassical Hartree-Fock-Popov description has produced excellent agreement with experimentally measured equilibrium quantities [7]. Further, unlike in a spatially homogeneous gas, it was found that collective elementary excitations contribute very little to thermodynamic properties [7] due to the relatively small spatial overlap between condensate and thermal component in a harmonic trap. Thus, even a semiclassical Hartree-Fock approximation is a fairly accurate description of these gases, except for a small temperature range close to the critical temperature. For example, excellent agreement has been achieved by a comparison of Hartree-Fock density profiles with the results of a comprehensive Path Integral Monte Carlo calculation [8].

In this paper we introduce a further simplification of the self-consistent Hartree-Fock model by neglecting atomic interactions in the thermal component of the gas. Like the introduction of the Thomas-Fermi approximation [5] the reduction to Eqs. (4)–(6) and (12) has the important advantage of providing an explicit analytical description of a trapped Bose gas at finite temperature.

We consider atoms that are trapped in a generally anisotropic harmonic potential. Under the appropriate rescaling of energy and lengths, the harmonic potential has the form $V(\mathbf{r}) = r^2/2$. Here, the dimensionless cartesian coordinates of $\mathbf{r}$ are given in units of $\sqrt{\hbar\omega/m\omega_{x,y,z}^2}$, with $\omega = (\omega_x\omega_y\omega_z)^{1/3}$. Other lengths, like the thermal wavelength λ_T and the scattering length a, are scaled in units of the natural length $\sqrt{\hbar/m\omega}$ of a harmonic oscillator with angular frequency ω. The energy $V(\mathbf{r})$ as well as other energies are implicitly given in units of $\hbar\omega$.

Then, in the self-consistent Hartree-Fock model, the densities of the condensate and the thermal component are given as solutions of the two coupled equations [5, 7]

$$n_0(\mathbf{r}) = \frac{\mu - r^2/2 - 2Un_T(\mathbf{r})}{U}\,\theta(\mu - r^2/2 - 2Un_T(r)) \quad (1)$$

$$n_T(\mathbf{r}) = \frac{1}{\lambda_T^3} g_{3/2}\left(e^{-(r^2/2+2U[n_0(\mathbf{r})+n_T(\mathbf{r})]-\mu)/k_BT}\right). \quad (2)$$

Here, the Thomas-Fermi approximation has been applied which neglects the kinetic energy of the condensate and implicitly finite size effects. The strength of the atomic interactions is given by $U = 4\pi a$. We use the thermal wavelength $\lambda_T = \sqrt{2\pi/k_BT}$ and the Bose function $g_{3/2}$ is defined by $g_\alpha(z) = \sum_{j=1}^{\infty} z^j/j^\alpha$. The chemical potential μ is determined by the constraint of a given total atom number

$$N = \int d\mathbf{r}\,[n_0(\mathbf{r}) + n_T(\mathbf{r})]. \quad (3)$$

For further reference, Eqs. (1) – (3) will be denoted as the interacting model. Even though it represents already a relatively concise description, these equations still have to be solved self-consistently. This is done numerically by an iterative procedure [7].

If one further neglects the mean-field repulsion from non-condensed atoms Eqs. (1) and (2) are solved by the explicit relations

$$n_0(\mathbf{r}) = \frac{\mu - r^2/2}{U}\,\theta(\mu - r^2/2) \tag{4}$$

$$n_T(\mathbf{r}) = \frac{1}{\lambda_T^3} g_{3/2}\left(e^{-|r^2/2-\mu|/k_BT}\right), \tag{5}$$

with the chemical potential μ given by

$$\mu = \frac{1}{2}(15Na)^{2/5}\left(\frac{N_0}{N}\right)^{2/5}. \tag{6}$$

These relations summarize a simple model of the partly condensed gas which we denote as the semi-ideal model. The condensate density n_0 is that of a zero temperature condensate with N_0 atoms, while the density n_T of the non-condensed cloud is that of an ideal gas of bosons confined in the combination of the external potential and the repulsive mean-field potential due to the condensate atoms. Its wide range of validity has been confirmed by a numerical analysis in Ref. [9]. However, in order to make it an intuitively appealing, usable description of a trapped Bose gas, the condensate fraction has to be determined analytically as a function of temperature.

For later convenience let us introduce the reduced chemical potential $\bar{\mu}$

$$\bar{\mu} = \frac{\mu}{k_BT} = \eta\left(\frac{N_0}{N}\right)^{2/5}\left(\frac{T}{T_c}\right)^{-1}. \tag{7}$$

Here, the critical temperature T_c is that of a trapped ideal gas [10, 11] $k_BT_c = [N/\zeta(3)]^{1/3}$ where $g_\alpha(1) = \zeta(\alpha)$ was expressed in terms of the Riemann Zeta function. The reduced chemical potential depends on the scaling parameter η [7]

$$\eta = \frac{\mu_{T=0}}{k_BT_c} = \frac{1}{2}\zeta(3)^{1/3}\left(15N^{1/6}a\right)^{2/5} \tag{8}$$

which describes the strength of the atomic interactions within the condensate. The scaling parameter is independent of the system size when the thermodynamic limit is taken in the usual way ($N \to \infty, \omega \to 0, N\omega^3 = \text{const.}$). Due to its relatively weak $N^{1/6}$ dependence, η assumes a value close to 0.3 in most recent experiments [7].

The condensate fraction is determined by integration over the thermal density distribution. For $T < T_c$, the result can be written in terms of incomplete Gamma functions [12]

$$\begin{aligned}\frac{N_0}{N} &= 1 - \frac{2}{\sqrt{\pi}}\frac{1}{\zeta(3)}\left(\frac{T}{T_c}\right)^3 \\ &\quad\times\sum_{j=1}^{\infty}\frac{1}{(jk_BT)^{3/2}}\left(\int_0^{\mu} d\epsilon\sqrt{\epsilon}\,e^{j(\epsilon-\mu)/k_BT}\right. \\ &\qquad\left. + \int_{\mu}^{\infty} d\epsilon\sqrt{\epsilon}\,e^{-j(\epsilon-\mu)/k_BT}\right) \\ &= 1 - \frac{2}{\sqrt{\pi}}\frac{1}{\zeta(3)}\left(\frac{T}{T_c}\right)^3\sum_{j=1}^{\infty}\frac{1}{j^3}\left[e^{-j\bar{\mu}}\gamma(3/2,-j\bar{\mu})\right. \\ &\qquad\left. + e^{j\bar{\mu}}\Gamma(3/2,j\bar{\mu})\right].\end{aligned} \tag{9}$$

Eq. (9) is still an implicit expression since it depends again on the reduced chemical potential. Therefore, $\bar{\mu}$ and N_0/N are given as simultaneous solutions of Eqs. (7) and (9). For temperatures $T > T_c$ a condensate does not exist and the reduced chemical potential $\bar{\mu} < 0$ is trivially defined by the single equation $g_3(e^{\bar{\mu}}) = \zeta(3)(T/T_c)^{-3}$.

Let us consider the results of the semi-ideal model in the limits of small and large $\bar{\mu}$, corresponding to $T \approx T_c$ and $T \approx 0$. Eq. (9) is therefore rewritten

$$\frac{N_0}{N} = 1 - \frac{2}{\sqrt{\pi}}\frac{1}{\zeta(3)}\left(\frac{T}{T_c}\right)^3\sum_{j=1}^{\infty}\frac{1}{j^3}f(j\bar{\mu}) \tag{10}$$

in terms of the function

$$f(x) = \int_0^x d\bar{\epsilon}\sqrt{\bar{\epsilon}}\,e^{\bar{\epsilon}-x} + \int_x^{\infty} d\bar{\epsilon}\sqrt{\bar{\epsilon}}\,e^{-(\bar{\epsilon}-x)}, \tag{11}$$

where the reduced energy $\bar{\epsilon} = \epsilon/k_BT$ has been introduced. The function $f(j\bar{\mu})$ can be expressed as a power series in $\sqrt{j\bar{\mu}}$, where $\bar{\mu}$ runs from 0 ($T = T_c$) to ∞ ($T = 0$). Truncating the series after the lowest nontrivial order yields

$$\begin{aligned}\frac{N_0}{N} &= 1 - \left(\frac{T}{T_c}\right)^3\left[1 + \frac{\zeta(2)}{\zeta(3)}\bar{\mu}\right] \\ &= 1 - \left(\frac{T}{T_c}\right)^3 - \eta\frac{\zeta(2)}{\zeta(3)}\left(\frac{T}{T_c}\right)^2\left(\frac{N_0}{N}\right)^{2/5}\end{aligned} \tag{12}$$

The first two terms of Eq. (12) correspond to the condensate fraction of an ideal gas, whereas the third describes the influence of the condensate repulsion to lowest order in $\bar{\mu}$. This expansion adequately describes the solution of Eq. (9) over the entire range of temperatures, provided that $\eta \ll 1$. A further simplification is derived by solving Eq. (12) to lowest order in η, arriving at

$$\frac{N_0}{N} = 1 - \left(\frac{T}{T_c}\right)^3 - \eta\frac{\zeta(2)}{\zeta(3)}\left(\frac{T}{T_c}\right)^2\left[1 - \left(\frac{T}{T_c}\right)^3\right]^{2/5}. \tag{13}$$

Within Eqs. (12) and (13), the only effect of the condensate interactions is to shift the chemical potential to positive values, raising the bottom of the effective potential which the thermal atoms experience. The effect of changing the shape of the potential enters only at higher orders of the expansion. Eq. (12) is thus a good approximation of Eq. (9) if most of the thermal atoms are spatially separated from the condensate, a condition satisfied for temperatures close to T_c and for small η.

Eq. (12) is not expected to be a good description for extremely low temperatures. The understanding of this limit is facilitated by $f(x)$ obeying the differential equation

$$\frac{d^2}{dx^2}f = f - 2\sqrt{x}. \tag{14}$$

The function $f(x)$ has to grow slower than $x^{3/2}$ for large values of x. Otherwise, the power series in Eq. (10) would not converge. As a consequence, the second derivative in Eq. (14) vanishes for large x. Thus, the asymptotic limit of the condensate fraction for low temperatures is given by $f(x) = 2\sqrt{x}$ or

$$\frac{N_0}{N} = 1 - \sqrt{\eta}\frac{4}{\sqrt{\pi}}\frac{\zeta(5/2)}{\zeta(3)}\left(\frac{T}{T_c}\right)^{5/2}. \qquad (15)$$

However, it has been shown [7] that the leading term of the uncondensed fraction around zero temperature scales like

$$\frac{N_0}{N} = 1 - \eta\frac{\pi^2}{2\sqrt{2}\,\zeta(3)}\left(\frac{T}{T_c}\right)^2 \qquad (16)$$

due to quasi-particle contributions which are included in neither the semi-ideal nor the interacting Hartree-Fock treatment.

According to Fig. 1, where $\eta = 0.31$ has been assumed, the high temperature expansions Eqs. (12) and to some extent Eq. (13) are very good approximations of the exact condensate fraction Eq. (9) of the semi-ideal model over the whole range of temperatures $T < T_c$. In contrast, we have found that the validity of the low temperature limits of Eqs. (15) and (16) are restricted to a very small range around zero temperature which makes them nearly irrelevant for practical purposes.

The condensate fraction given by the approximate solution of the semi-ideal model in Eq. (12) is compared in Fig. 2 with the result of an iterative solution of the interacting model (Eqs. (1)–(3)). The difference between the curves is small except near the critical temperature, where the interactions among thermal atoms shift the critical temperature [13]. This shift is not exhibited by the semi-ideal model. The wide range of validity of the semi-ideal model has also been confirmed by a numerical comparison with a Hartree-Fock-Popov calculation [9]. The latter includes collective excitations, which are ignored in the models shown in Fig. 2. These lead to an additional but negligible decrease of the condensate fraction [7].

A direct comparison between the density distributions of the different models is given in Fig. 3 for $T/T_c = 0.5$. Here, the Thomas-Fermi solution of the condensate density of Eq. (1) has been replaced by a solution of the full Gross-Pitaevskii equation. The main implication of the included kinetic energy of the condensate is a smoothed out condensate surface. Within the Thomas-Fermi approximation almost no difference is seen between the two curves. Even though the unaccounted existence of collective excitations changes the densities of condensate and thermal component close to the center of the trap by a significant amount, their influence on the total density is negligibly small for most temperatures [8].

In recent experiments, trapped Bose gases have been probed in-situ using either non-destructive dispersive imaging techniques [14], or off-resonant absorption imaging [15]. These methods are important new tools in the understanding of trapped Bose gases, with distinct advantages over the previously used time of flight measurements of expanding atom clouds [1, 2]. We therefore expect that the results of this paper will become useful for future in-situ experiments with trapped Bose gases. These new optical detection techniques measure column or line density profiles; we therefore determine these profiles from Eqs. (4) and (5) by integration over one or two dimensions.

In cylindrical coordinates, where the probe beam is directed along the z-axis, the according column densities are given by

$$n_0(\rho) = \frac{4\sqrt{2}}{3}\frac{(\mu - \rho^2/2)^{3/2}}{U}\,\theta(\mu - \rho^2/2) \qquad (17)$$

$$n_T(\rho) = \frac{2\pi}{\lambda_T^4}\begin{cases} g_2(e^{\bar{\mu}(\rho)}) & \bar{\mu}(\rho) < 0 \\ \int_0^\infty d\bar{\epsilon}\,\frac{1}{\sqrt{\pi\bar{\epsilon}}}\,g_{3/2}(e^{-|\bar{\epsilon}-\bar{\mu}(\rho)|}) & \bar{\mu}(\rho) > 0 \end{cases} \qquad (18)$$

where $\bar{\mu}(\rho) = (\mu - \rho^2/2)/k_BT$. Equivalently, we obtain the line densities

$$n_0(z) = \pi\frac{(\mu - z^2/2)^2}{U}\,\theta(\mu - z^2/2) \qquad (19)$$

$$n_T(z) = \frac{(2\pi)^2}{\lambda_T^5}\begin{cases} g_{5/2}(e^{\bar{\mu}(z)}) & \bar{\mu}(z) < 0 \\ 2\zeta(5/2) - g_{5/2}(e^{-\bar{\mu}(z)}) & \bar{\mu}(z) > 0 \end{cases} \qquad (20)$$

with $\bar{\mu}(z) = (\mu - z^2/2)/k_BT$.

We therefore conclude that the proposed semi-ideal model of Eqs. (4)–(6) and (12) represents a rather good description of a trapped Bose gas at finite temperature provided that η is not larger than the values $\eta \approx 0.3$ to 0.4 achieved in recent experiments. Its mathematical simplicity gives a much clearer conceptual picture than the self-consistent approaches that have been used before. The observed agreement of the semi-ideal model with a self-consistent Hartree-Fock calculation has confirmed that the density of the thermal component is too low to necessitate an interacting gas description. Instead, the observed depletion of the condensate fraction arises from condensate interactions, leading to a positive value of the chemical potential or equivalently to a raised bottom of the effective potential in which the thermal component resides. It is well described by Eq. (12), which is a low order expansion in $\bar{\mu}$. In contrast, the changed shape of the effective potential does not influence the thermal population in a noticeable way.

This work was supported by the Deutsche Forschungsgemeinschaft (DFG) and also the Office of Naval Research, the Joint Services Electronics Program (ARO) and the JSEP Graduate Fellowship Program. It is a pleasure to thank M. Olshanii, H.-J. Miesner, and W. Ketterle for many valuable discussions. After the completion of this work, E. Mueller brought to our attention a numerical calculation of the condensate fraction within the semi-ideal model [16].

[1] M. H. Anderson *et al.*, Science **269**, 198 (1995).
[2] K. B. Davis *et al.*, Physical Review Letters **75**, 3969 (1995).
[3] E. P. Gross, Nuovo Cimento **20**, 454 (1961).
[4] L. P. Pitaevskii, Sov. Phys. JETP **13**, 451 (1961).
[5] V. V. Goldman, I. F. Silvera, and A. J. Leggett, Physical Review B **24**, 2870 (1981).
[6] G. Baym and C. J. Pethick, Physical Review Letters **76**, 6 (1996).
[7] S. Giorgini, L. P. Pitaevskii, and S. Stringari, Journal of Low Temperature Physics **109**, 309 (1997).
[8] M. Holzmann, W. Krauth, and M. Naraschewski, (unpublished).
[9] R. J. Dodd, K. Burnett, M. Edwards, and C. W. Clark, (unpublished).
[10] V. Bagnato, D. E. Pritchard, and D. Kleppner, Physical Review A **35**, 4354 (1987).
[11] W. Ketterle and N. J. van Druten, Physical Review A **54**, 656 (1996).
[12] I. S. Gradshteyn and I. M. Ryzhik, *Table of Integrals, Series, and Products*, 4 ed. (Academic Press, London, 1980).
[13] S. Giorgini, L. P. Pitaevskii, and S. Stringari, Physical Review A **54**, R4633 (1996).
[14] M. R. Andrews *et al.*, Science **273**, 84 (1996).
[15] L. V. Hau *et al.*, (unpublished).
[16] A. Minguzzi, S. Conti, and M. P. Tosi, Journal of Physics: Condensed Matter **9**, L33 (1997).

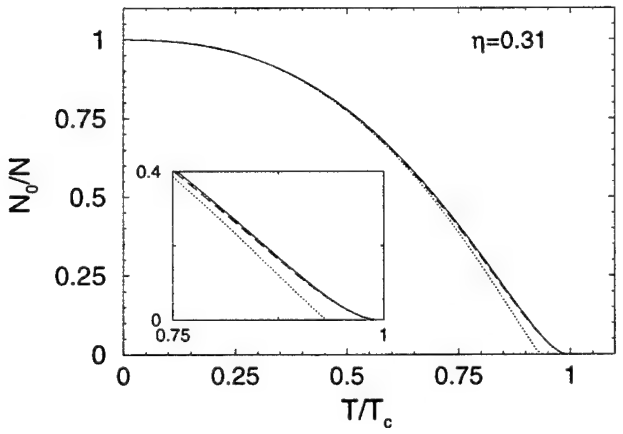

FIG. 1. Condensate fraction as a function of temperature, given by the semi-ideal model. The dashed line shows the exact solution Eq. (9) of the semi-ideal model. The solid line represents its high-temperature limit Eq. (12). The explicit expression of Eq. (13) is given by the dotted line. This plot demonstrates the validity of Eq. (12) over the whole range of temperatures $T < T_c$. The explicit approximation of Eq. (13) fails only in the vicinity of the critical temperature (shown in the inset).

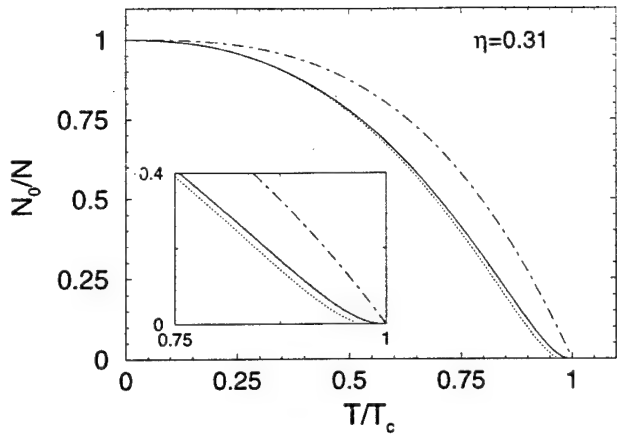

FIG. 2. Condensate fraction plotted as a function of temperature, comparing the discussed models. The ideal gas condensate fraction is given by the dashed-dotted line. The dotted line is a numerical solution of the Hartree-Fock Eqs. (1)–(3). The solid line is obtained from the analytical approximation Eq. (12), corresponding to the solid line of Fig. 1. Except near the critical temperature (shown in the inset), the semi-ideal model well approximates the solution of the interacting model. The critical temperature T_c refers to the case of an ideal gas.

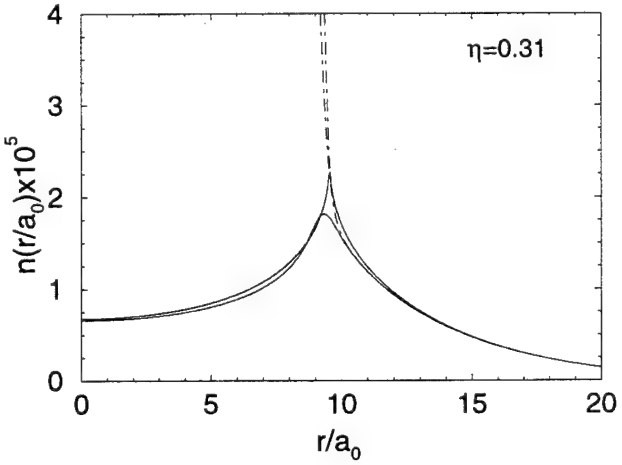

FIG. 3. A comparison of the density distributions at $T/T_c = 0.5$ predicted by the two discussed models. The upper solid line shows the density of the thermal component as given by Eq. (5). In comparison, the lower solid line has been calculated numerically using Eq. (2). However, a numerical solution of the full Gross-Pitaevskii equation has been used instead of the Thomas-Fermi approximation of Eq. (1). A small difference exists at the edge of the condensate due to the neglect of the kinetic energy in the semi-ideal model. However, the total density is only weakly affected by this effect, as is seen by the two dashed-dotted lines. Again, the upper dashed-dotted line refers to the total density given by the semi-ideal model while the lower curve corresponds to the self-consistent Hartree-Fock approximation. Here, a total atom number of $N = 5 \times 10^6$ was assumed.

Observation of Feshbach resonances in a Bose–Einstein condensate

S. Inouye*, M. R. Andrews*†, J. Stenger*, H.-J. Miesner*, D. M. Stamper-Kurn* & W. Ketterle*

* Department of Physics and Research Laboratory of Electronics, Massachusetts Institute of Technology, Cambridge, Massachusetts 02139, USA

It has long been predicted that the scattering of ultracold atoms can be altered significantly through a so-called 'Feshbach resonance'. Two such resonances have now been observed in optically trapped Bose–Einstein condensates of sodium atoms by varying an external magnetic field. They gave rise to enhanced inelastic processes and a dispersive variation of the scattering length by a factor of over ten. These resonances open new possibilities for the study and manipulation of Bose–Einstein condensates.

Bose–Einstein condensates of atomic gases offer new opportunities for studying quantum-degenerate fluids[1–5]. All the essential properties of Bose condensed systems—the formation and shape of the condensate, the nature of its collective excitations and statistical fluctuations, and the formation and dynamics of solitons and vortices—are determined by the strength of the atomic interactions. In contrast to the situation for superfluid helium, these interactions are weak, allowing the phenomena to be theoretically described from 'first principles'. Furthermore, in atomic gases the interactions can be altered, for instance by employing different species, changing the atomic density, or, as in the present work, merely by varying a magnetic field.

At low temperatures, the interaction energy in a cloud of atoms is proportional to the density and a single atomic parameter, the scattering length a which depends on the quantum-mechanical phase shift in an elastic collision. It has been predicted that the scattering length can be modified by applying external magnetic[6–10], optical[11,12] or radio-frequency[13] (r.f.) fields. Those modifications are only pronounced in a so-called "Feshbach resonance"[14], when a quasibound molecular state has nearly zero energy and couples resonantly to the free state of the colliding atoms. In a time-dependent picture, the two atoms are transferred to the quasibound state, 'stick' together and then return to an unbound state. Such a resonance strongly affects the scattering length (elastic channel), but also affects inelastic processes such as dipolar relaxation[6,7] and three-body recombination. Feshbach resonances have so far been studied at much higher energies[15] by varying the collision energy, but here we show that they can be 'tuned' to zero energy to be resonant for ultracold atoms. The different magnetic moments of the free and quasibound states allowed us to tune these resonances with magnetic fields, and as a result, minute changes in the magnetic field strongly affected the properties of a macroscopic system.

Above and below a Feshbach resonance, the scattering length a covers the full continuum of positive and negative values. This should allow the realization of condensates over a wide range of interaction strengths. By setting $a \approx 0$, one can create a condensate with essentially non-interacting atoms, and by setting $a < 0$ one can make the system unstable and observe its collapse. Rapid tuning of an external magnetic field around a Feshbach resonance will lead to sudden changes of the scattering length. This opens the way to studies of new dynamical effects such as novel forms of collective oscillations or the sudden collapse of a large condensate when the scattering length is switched from positive to negative[16].

† Present address: Bell Laboratories, Lucent Technologies, Murray Hill, New Jersey 07974, USA.

Theoretical predictions

Calculations for Feshbach resonances in external magnetic fields have been reported for the lower hyperfine states of the atoms Li (ref. 8), K (ref. 10), Na (ref. 8), Rb (ref. 9) and Cs (refs 6, 7). They are typically spaced by several hundred gauss, and for Li and Na occur outside the range where states in the lower hyperfine manifold are weak-field-seeking and can be magnetically trapped. Recent experimental efforts to observe Feshbach resonances have concentrated on ^{87}Rb (ref. 17) and on ^{85}Rb (ref. 18 and C. E. Wieman, personal communication) where Feshbach resonances have been predicted at relatively low magnetic fields[9]. However, our recently demonstrated all-optical confinement of a Bose condensate[19] opened the possibility of observing Feshbach resonances for strong-field-seeking states which cannot be trapped in a d.c. magnetic trap. The optical trapping potential is unaffected by magnetic fields and is independent of the hyperfine ground state. We report here the observation of two Feshbach resonances of sodium in a strong-field-seeking state.

Several Feshbach resonances in sodium are caused by quasibound hyperfine states of the second highest vibrational level, $v = 14$, of the triplet potential of the sodium dimer. The lowest magnetic field value B_0 for a strong Feshbach resonance in sodium was predicted to lie in the range $760 < B_0 < 925$ G (B. J. Verhaar and F. A. van Abeelen, personal communication). It occurs in collisions between atoms in the lowest hyperfine state $|m_S = -1/2, m_I = +3/2\rangle$, which correlates with the $|F = 1, m_F = +1\rangle$ state at low fields (S, I and F are the usual quantum numbers for the electronic, nuclear and total spin, respectively). This Feshbach resonance is due to a quasibound molecular state $|S = 1, m_S = +1, I = 1, m_I = +1\rangle$. A much weaker resonance due to a $|S = 1, m_S = +1, I = 3, m_I = +1\rangle$ state (which is almost degenerate with the other quasibound state) was predicted to occur 50 to 75 G below.

Near a Feshbach resonance, the scattering length a should vary dispersively as a function of magnetic field B (ref. 8):

$$a = \tilde{a}\left(1 - \frac{\Delta}{B - B_0}\right) \qquad (1)$$

where Δ parametrizes the width of the resonance at $B = B_0$, and $\tilde{a}$ is the scattering length outside the resonance. For sodium, $\tilde{a}$ was found spectroscopically to be 2.75 nm at zero field, and increases to the triplet scattering length of 4.5 nm (ref. 20) at high magnetic fields. The widths Δ for the strong and weak resonance were predicted to be 1 G and 0.01 G, respectively (B. J. Verhaar and F. A. van Abeelen, personal communication).

Experimental set-up

Bose–Einstein condensates in the $|F = 1, m_F = -1\rangle$ state were produced as in our previous work by laser cooling, followed by evaporative cooling in a magnetic trap[21]. The condensates were transferred into an optical dipole trap formed at the focus of an infrared laser beam[19]. Atoms were then spin-flipped with nearly 100% efficiency to the $|F = 1, m_F = +1\rangle$ state with an adiabatic r.f. sweep while applying a 1 G bias field. Without large modifications of our magnetic trapping coils, we could provide bias fields of up to ~1,200 G, but only by using coils producing axial curvature[21], which for high-field-seeking states generated a repulsive axial potential. At the highest magnetic fields, this repulsion was stronger than the axial confinement provided by the optical trap. To prevent the atoms from escaping, two 'end-caps' of far-off-resonant blue-detuned laser light were placed at the ends of the condensate, creating a repulsive potential, and confining the atoms axially (Fig. 1a). For this, green light at 514 nm from an argon-ion laser was focused into two sheets about 200 μm apart. The focus of the optical trap was placed near the minimum of the bias field in order to minimize the effect of the destabilizing magnetic field curvature. The axial trapping potential at high fields was approximately "W"-shaped (Fig. 1b), and had a minimum near one of the end-caps as observed by phase-contrast imaging[22] (Fig. 1c, d).

The calibration factor between the current (up to ~400 A) in the coils and the magnetic bias field was determined with an accuracy of 2% by inducing r.f. transitions within the $|F = 1\rangle$ ground-state hyperfine manifold at about 40 G. Additionally, an optical resonance was found around 1,000 G, where the Zeeman shift equalled the probe light detuning of about 1.7 GHz and led to a sign-reversal of the phase-contrast signal. These two calibrations agreed within their uncertainties.

The condensate was observed in the trap directly using phase-contrast imaging[22] or by using time-of-flight absorption imaging[1,2,21]. In the latter case, the optical trap was suddenly switched off, and the magnetic bias field was shut off 1–2 ms later to ensure that the high-field value of the scattering length was responsible for the acceleration of the atoms. After ballistic expansion of the condensate (either 12 or 20 ms), the atoms were optically pumped into the $|F = 2\rangle$ ground state and probed using resonant light driving the cycling transition. The disk-like expansion of the cloud and the radial parabolic density profile were clear evidence for the presence of a Bose condensed cloud.

Locating the resonances

When the magnetic field is swept across a Feshbach resonance one would expect to lose a condensate due to an enhanced rate of inelastic collisions (caused either by the collapse in the region of negative scattering length or by an enhanced rate coefficient for inelastic collisions). This allowed us to implement a simple procedure to locate the resonances: we first extended the field ramp until the atoms were lost and then used successively narrower field intervals to localize the loss. This procedure converged much faster than a point-by-point search. As we could take many non-destructive phase-contrast images during the magnetic field ramp, the sharp onset of trap loss at the resonance was easily monitored (Fig. 1c, d).

The most robust performance was obtained by operating the optical dipole trap at 10 mW laser power focused to a beam waist of 6 μm, resulting in tight confinement of the condensate and therefore rather short lifetimes owing to three-body recombination[19]. This required that the magnetic field be ramped up in two stages: a fast ramp at a rate of ~100 G ms^{-1} to a value slightly below that expected for a Feshbach resonance, followed by a slow ramp at a rate between 0.05 and 0.3 G ms^{-1} to allow for detailed observation. Near 907 G, we observed a dramatic loss of atoms, as shown in Figs 1c and 2a. This field value was reproducible to better than 0.5 G and had a calibration uncertainty of ±20 G.

To distinguish between an actual resonance and a threshold for trap loss, we also approached the resonance from above. Fields above the Feshbach resonance were reached by ramping at a fast rate of 200 G ms^{-1}, thus minimizing the time spent near the resonance and the accompanying losses. The number of atoms above the resonance was typically three times smaller than below. Approaching the resonance from above, a similarly sharp loss phenomenon was observed about 1 G higher in field than from below (Fig. 2a), which roughly agrees with the predicted width of the resonance. A second resonance was observed 54 ± 1 G below the first one, with the observed onset of trap loss at least a factor of ten sharper than for the first. As the upper resonance was only reached by passing through the lower one, some losses of atoms were unavoidable; for example, when the lower resonance was crossed at 2 G ms^{-1},

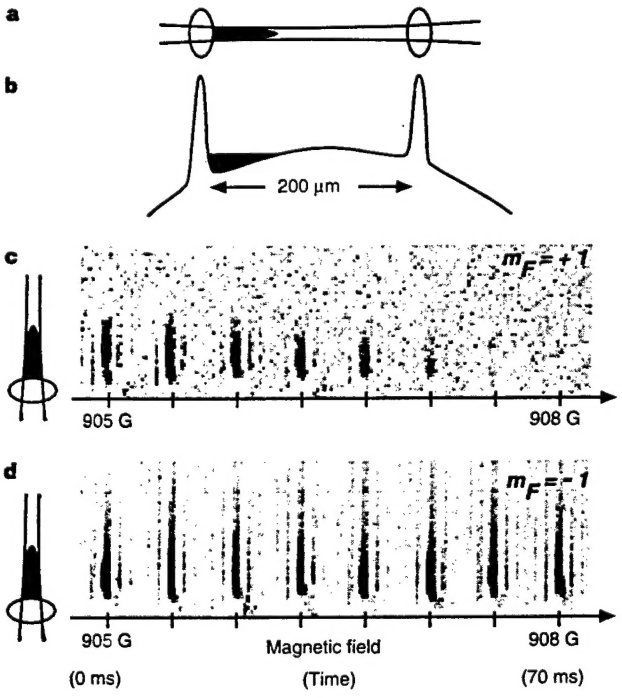

Figure 1 Observation of the Feshbach resonance at 907 G using phase-contrast imaging in an optical trap. A rapid sequence (100 Hz) of non-destructive, *in situ* phase-contrast images of a trapped cloud (which appears black) is shown. As the magnetic field was increased, the cloud suddenly disappeared for atoms in the $|m_F = +1\rangle$ state (see images in **c**), whereas nothing happened for a cloud in the $|m_F = -1\rangle$ state (images in **d**). The height of the images is 140 μm. A diagram of the optical trap is shown in **a**. It consisted of one red-detuned laser beam providing radial confinement, and two blue-detuned laser beams acting as end-caps (shown as ovals). The minimum of the magnetic field was slightly offset from the centre of the optical trap. As a result, the condensate (shaded area) was pushed by the magnetic field curvature towards one of the end-caps. The axial profile of the total potential is shown in **b**.

about 80% of the atoms were lost. This, coupled with the stability and finite programming speed of the power supplies, limited the ramp rates to those given above.

The observation of twin resonances separated by 54 ± 1 G, with the weaker one at lower field, exactly matches the theoretically predicted pattern and thus strongly confirms our interpretation. No resonance phenomena were observed in the $|m_F = -1\rangle$ state at any field up to 1,000 G, in agreement with theory which predicted resonances for this state only at much higher fields.

Changing the scattering length

The trap loss measurements easily located the Feshbach resonances. To measure the variation of the scattering length around these resonances, we determined the interaction energy of a trapped condensate. This was done by suddenly switching off the trap, allowing the stored interaction energy to be converted into the kinetic energy of a freely expanding condensate and measuring it by time-of-flight absorption imaging[1,2,21]. The interaction energy is proportional to the scattering length and the average density of the condensate $\langle n \rangle$:

$$E_I/N = \frac{2\pi\hbar^2}{m} a \langle n \rangle \qquad (2)$$

where N is the number of condensed atoms of mass m. For a large condensate the kinetic energy in the trap is negligible (Thomas–Fermi limit), and E_I is equal to the kinetic energy E_K of the freely expanding condensate $E_K/N = mv_{rms}^2/2$, where v_{rms} is the root-mean-square velocity of the atoms. For a three-dimensional harmonic oscillator potential one finds $\langle n \rangle \propto N(Na)^{-3/5}$ (ref. 23) (We note that, for a general power-law potential $\Sigma_i c_i x_i^{p_i}$, one obtains $\langle n \rangle \propto N(Na)^{k-1}$, where $k = 1/(1 + \Sigma_i 1/p_i)$). Thus, the value of the scattering length scales as:

$$a \propto \frac{v_{rms}^5}{N} \qquad (3)$$

Both v_{rms} and N can be directly evaluated from absorption images of freely expanding condensates. For a cigar-shaped condensate the free expansion is predominantly radial, and so the contribution of the axial dimension to v_{rms} could be neglected. The quantity v_{rms}^5/N (equation (3)), normalized to unity outside the resonance, should be identical to $a/\bar{a}$ (equation (1)). This quantity was measured around the resonance at 907 G and is shown in Fig. 2b together with the theoretical prediction of a resonance with width $\Delta = 1$ G. The data clearly displays the predicted dispersive shape and shows evidence for a variation in the scattering length by more than a factor of ten.

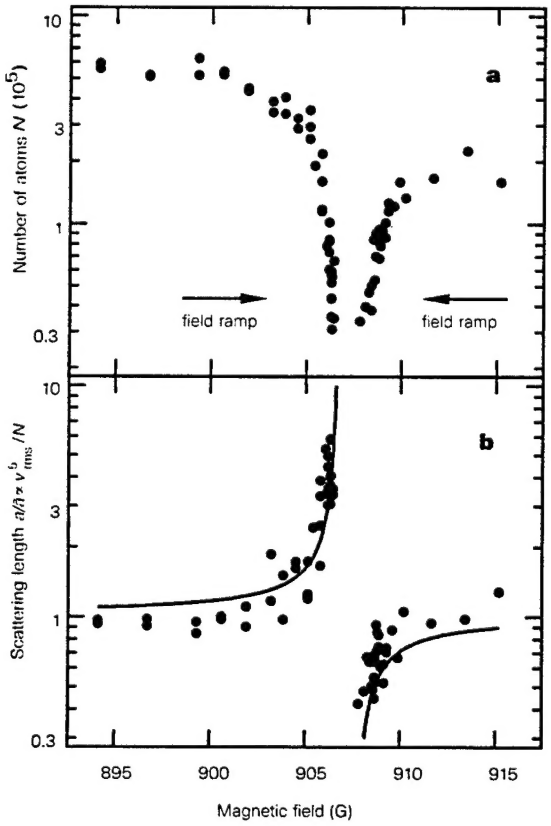

Figure 2 Observation of the Feshbach resonance at 907 G using time-of-flight absorption imaging. **a**, Number of atoms in the condensate versus magnetic field. Field values above the resonance were reached by quickly crossing the resonance from below and then slowly approaching from above. **b**, The normalized scattering length $a/\bar{a} \propto v_{rms}^5/N$ calculated from the released energy, together with the predicted shape (equation (1), solid line). The values of the magnetic field in the upper scan relative to the lower one have an uncertainty of <0.5 G.

We now discuss the assumptions for equation (3) and show that it is approximately valid for our conditions. (1) We assumed that the condensate remains in equilibrium during the magnetic field ramp. This is the case if the adiabatic condition $\dot{a}/a \ll \omega_i$ holds for the temporal change of the scattering length[16], and a similar condition for the loss of atoms (the ω_i are the trapping frequencies). For the condensate's fast radial dynamics ($\omega_r \approx 2\pi \times 1.5$ kHz) this condition is fulfilled, whereas for the slower axial motion ($\omega_z \approx 2\pi \times 0.1$ kHz) it breaks down close to or within the resonance. In this case the density would approach the two-dimensional scaling $N(Na)^{-1/2}$, but the values for $a/\bar{a}$ (Fig. 2b) would differ by at most 50%. (2) The second assumption was a three-dimensional harmonic trap. If the axial potential has linear contributions, the density scales instead like $N(Na)^{-2/3}$ resulting in at most a 50% change for $a/\bar{a}$. (3) We assumed that contributions of collective excitations to the released energy were small. Axial striations were observed in free expansion for both $|m_F = +1\rangle$ and $|m_F = -1\rangle$ atoms (probably created by the changing potential during the fast magnetic field ramp). However, the small scatter of points outside the resonance in Fig. 2b, which do not show any evidence of oscillations, suggests that the contribution of excitations to the released energy is negligible. (4) We assumed a sudden switch-off of the trap and ballistic expansion. The inhomogeneous bias field during the first 1–2 ms of free expansion accelerated the axial expansion, but had a negligible effect on the expansion of the condensate in the radial direction, which was evaluated for Fig. 2b.

None of the corrections (1)–(4) discussed above affect our conclusion that the scattering length varies dispersively near a Feshbach resonance. More accurate experiments should be done with a homogeneous bias field. In addition, an optical trap with larger volume and lower density would preclude the need to ramp the field quickly because three-body recombination would be reduced.

The trap losses observed around the Feshbach resonances merit further study as they might impose practical limits on the possibilities for varying the scattering length. An increase of the dipolar relaxation rate near Feshbach resonances has been predicted[6,7], but for atoms in the lowest hyperfine state no such inelastic binary collisions are possible. Therefore, the observed trap loss is probably due to three-body collisions. In this case the loss rate is characterized by the coefficient K_3, defined as $\dot{N}/N = -K_3\langle n^2 \rangle$. So far, there is no theoretical work on K_3 near a Feshbach resonance. An analysis based on Fig. 2 shows that K_3 increased on both sides of the resonance, because the loss rate increased while the density decreased or stayed constant. In any case, the fact that we observed Feshbach resonances at high atomic densities ($\sim 10^{15}$ cm^{-3}) strongly enhanced this loss process, which can be avoided with a condensate at lower density in a modified optical trap. Control of the bias field with a precision better than $\sim 10^{-4}$ will be necessary to achieve negative or extremely large values of the scattering length in a stable way.

A tunable condensate

We have observed two Feshbach resonances for Bose–Einstein condensates of sodium through the abrupt loss of atoms, and obtained strong evidence for a dispersive variation of the scattering length by a factor of more than ten. 'Tuning' of the scattering length should become an important tool for 'designing' atomic quantum gases with novel properties; for example, to create ideal Bose–Einstein condensates with nearly zero scattering length, and to obtain a detailed picture of the collapse of a condensate with negative scattering length, which is so far not fully understood. Tuning the scattering length can also be used to vary interactions between different species[24] and thus control the phase diagram of multi-component condensates, possibly switching from interpenetrating superfluids to phase separation[25]. Feshbach resonances may also be important in atom optics, for modifying the atomic interactions in an atom laser, or more generally, for controlling nonlinear coefficients in atom optics with coherent beams of atoms. □

Received 18 February; accepted 19 February 1998.

1. Anderson, M. H., Ensher, J. R., Matthews, M. R., Wieman, C. E. & Cornell, E. A. Observation of Bose-Einstein condensation in a dilute atomic vapor. *Science* **269,** 198–201 (1995).
2. Davis, K. B. *et al.* Bose-Einstein condensation in a gas of sodium atoms. *Phys. Rev. Lett.* **75,** 3969–3973 (1995).
3. Bradley, C. C., Sackett, C. A. & Hulet, R. G. Bose-Einstein condensation of lithium: Observation of limited condensate number. *Phys. Rev. Lett.* **78,** 985–989 (1997).
4. Georgia Southern University BEC home page, http://amo.phy.gasou.edu/bec.html.
5. Bradley, C. C., Sackett, C. A., Tollett, J. J. & Hulet, R. G. Evidence of Bose-Einstein condensation in an atomic gas with attractive interactions. *Phys. Rev. Lett.* **75,** 1687–1690 (1995).
6. Tiesinga, E., Moerdijk, A. J., Verhaar, B. J. & Stoof, H. T. C. Conditions for Bose-Einstein condensation in magnetically trapped atomic cesium. *Phys. Rev. A* **46,** R1167–R1170 (1992).
7. Tiesinga, E., Verhaar, B. J. & Stoof, H. T. C. Threshold and resonance phenomena in ultracold ground-state collisions. *Phys. Rev. A* **47,** 4114–4122 (1993).
8. Moerdijk, A. J., Verhaar, B. J. & Axelsson, A. Resonances in ultracold collisions of ^{6}Li, ^{7}Li and ^{23}Na. *Phys. Rev. A* **51,** 4852–4861 (1995).
9. Vogels, J. M. *et al.* Prediction of Feshbach resonances in collisions of ultracold rubidium atoms. *Phys. Rev. A* **56,** R1067–R1070 (1997).
10. Boesten, H. M. J. M., Vogels, J. M., Tempelaars, J. G. C. & Verhaar, B. J. Properties of cold collisions of ^{39}K atoms and of ^{41}K atoms in relation to Bose-Einstein condensation. *Phys. Rev. A* **54,** R3726–R3729 (1996).
11. Fedichev, P. O., Kagan, Yu., Shlyapnikov, G. V. & Walraven, J. T. M. Influence of nearly resonant light on the scattering length in low-temperature atomic gases. *Phys. Rev. Lett.* **77,** 2913–2916 (1996).
12. Bohn, J. L. & Julienne, P. S. Prospects for influencing the scattering lengths with far-off-resonant light. *Phys. Rev. A* **56,** 1486–1491 (1997).
13. Moerdijk, A. J., Verhaar, B. J. & Nagtegaal, T. M. Collisions of dressed ground-state atoms. *Phys. Rev. A* **53,** 4343–4351 (1996).
14. Feshbach, H. A unified theory of nuclear reactions. II. *Ann. Phys.* **19,** 287–313 (1962).
15. Bryant, H. C. *et al.* Observation of resonances near 11 eV in the photodetachment cross-section of the H^- ion. *Phys. Rev. Lett.* **38,** 228–230 (1977).
16. Kagan, Yu., Surkov, E. L. & Shlyapnikov, G. V. Evolution and global collapse of trapped Bose condensates under variations of the scattering length. *Phys. Rev. Lett.* **79,** 2604–2607 (1997).
17. Newbury, N. R., Myatt, C. J. & Wieman, C. E. s-wave elastic collisions between cold ground-state ^{87}Rb atom. *Phys. Rev. A* **51,** R2680–R2683 (1995).
18. Courteille, P. & Heinzen, D. Paper presented at *SPIE Photonics West,* **24–30** Jan., San Jose, California (1998).
19. Stemper-Kurn, D. M. *et al.* Optical confinement of a Bose-Einstein condensate. *Phys. Rev. Lett.* (in the press).
20. Tiesinga, E. *et al.* A spectroscopic determination of scattering lengths for sodium atom collisions. *J. Res. Natl Inst. Stand. Technol.* **101,** 505–520 (1996).
21. Mewes, M.-O. *et al.* Bose-Einstein condensation in a tightly confining d.c. magnetic trap. *Phys. Rev. Lett.* **77,** 416–419 (1996).
22. Andrews, M. R. *et al.* Propagation of sound in a Bose–Einstein condensate. *Phys. Rev. Lett.* **79,** 553–556 (1997).
23. Baym, G. & Pethick, C. J. Ground-state properties of magnetically trapped Bose-condensed rubidium gas. *Phys. Rev. Lett.* **76,** 6–9 (1996).
24. van Abeelen, F. A., Verhaar, B. J. & Moerdijk, A. J. Sympathetic cooling of ^{6}Li atoms. *Phys. Rev. A* **55,** 4377–4381 (1997).
25. Ho, T.-L. & Shenoy, V. B. Binary mixtures of Bose condensates of alkali atoms. *Phys. Rev. Lett.* **77,** 3276–3279 (1996).

Acknowledgements. We thank J. M. Vogels for discussions, A. P. Chikkatur for experimental assistance, and B. J. Verhaar and F. A. van Abeelen for providing updated theoretical predictions. We also thank D. Kleppner, D. E. Pritchard and R. A. Rubenstein for a critical reading of the manuscript. This work was supported by the Office of Naval Research, NSF, Joint Services Electronics Program (ARO), and the David and Lucile Packard Foundation. J.S. acknowledges support from the Alexander von Humboldt-Foundation, and D.M.S.-K. was supported by the JSEP graduate fellowship program.

Correspondence and requests for materials should be addressed to W.K.

ATTACHMENT NUMBER 1

REPORTS AND REPORT DISTRIBUTION

REPORT TYPES

(a) Performance (Technical) Report(s) (Include letter report(s)) Frequency: Annual

(b) Final Technical Report, issued at completion of Grant.
NOTE: Final Technical Reports must have a SF-298 accompanying them. Unless otherwise stated in the grant, complete Block 12a. of the SF-298: "Approved for Public Release; distribution is Unlimited."

(c) Final Financial Status Report (SF 269)

(d) Final Patent Report (DD 882)

REPORTS DISTRIBUTION		
ADDRESSEES	**REPORT TYPES**	**NUMBER OF COPIES**
Office of Naval Research Program Officer Colin E. Wood ONR 312 Ballston Centre Tower One 800 North Quincy Street Arlington, VA 22217-5660	(a) & (b) w/(SF-298's)	3
Administrative Grants Officer OFFICE OF NAVAL RESEARCH REGIONAL OFFICE BOSTON * 495 SUMMER STREET ROOM 103 BOSTON, MA 02210-2109	(c), (d) & SF-298's only for (a) & (b)	1
Director, Naval Research Laboratory Attn: Code 5227 4555 Overlook Drive Washington, DC 20375-5326	(a) & (b) w/(SF-298's)	1
Defense Technical Information Center 8725 John J. Kingman Road STE 0944 Ft. Belvoir, VA 22060-6218	(a) & (b) w/(SF-298's)	2
Office of Naval Research Attn: ONR 00CC1 Ballston Centre Tower One 800 North Quincy Street Arlington, VA 22217-5660	(d)	1

If the Program Officer directs, the Grantee shall make additional distribution of technical reports in accordance with a supplemental distribution list provided by the Program Officer. The supplemental distribution list shall not exceed 250 addresses.

* For report types (a) and (b), send only a copy of the transmittal letter to the Administrative Contracting Officer; do not send actual reports to the Administrative Contracting Officer.